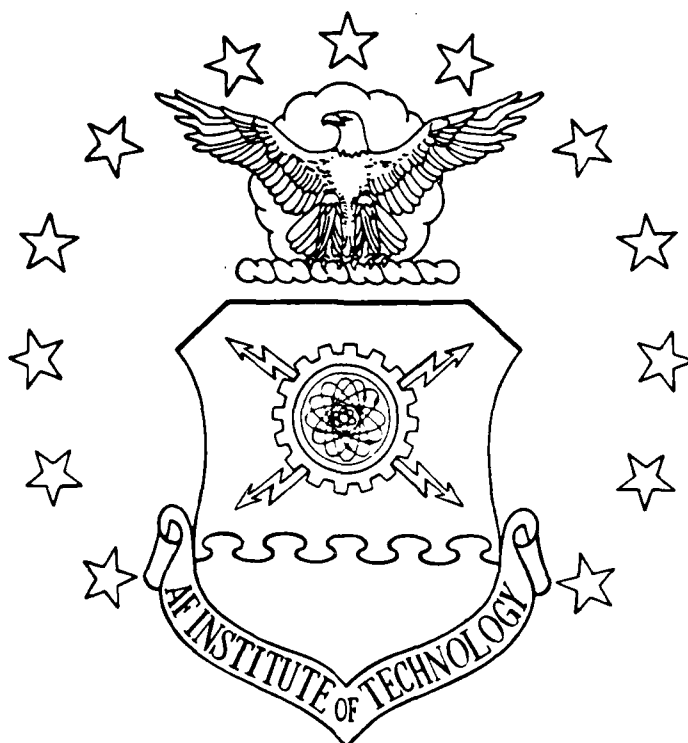MICROCOPY RESOLUTION TEST CHART
NATIONAL BUREAU OF STANDARDS-1963

AD-A189 716

NONLINEAR OPTICAL PHASE

CONJUGATION IN FLUORESCEIN

AND BISMUTH SILICATE (BSO)

THESIS

Phillip R. Leatherman
Captain, USAF
ENP

DEPARTMENT OF THE AIR FORCE

AIR UNIVERSITY

AIR FORCE INSTITUTE OF TECHNOLOGY

Wright-Patterson Air Force Base, Ohio
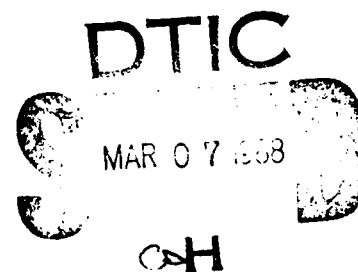
88 3 01 081

$\stackrel{ENP}{AFIT/GEO/\overline{PHY}/87D-2}$

NONLINEAR OPTICAL PHASE

CONJUGATION IN FLUORESCEIN

AND BISMUTH SILICATE (BSO)

THESIS

Phillip R. Leatherman
Captain, USAF
$\stackrel{ENP}{AFIT/GEO/\overline{PHY}/87D-2}$

DTIC

MAR 0 7 1988

C&H

NONLINEAR OPTICAL PHASE CONJUGATION

IN FLUORESCEIN AND BISMUTH SILICATE (BSO)

THESIS

Presented to the Faculty of the School of Engineering

of the Air Force Institute of Technology

Air University

In Partial Fulfillment of the

Requirements for the Degree of

Master of Science in Electrooptics

Phillip R. Leatherman, B.A., B.S.

Captain, USAF

December 1987

Preface

The work performed in this thesis was an initial study
of nonlinear optical phase conjugation (NOPC) at the Air
Force Institute of Technology, School of Engineering, Physics
Department. The investigation of parameters that affect NOPC
in BSO and fluorescein-doped boric acid glass hopefully will
provide the background needed for future work in NOPC
applications.

I thank Dr. W. B. Roh, Dr. Ted Luke, Major D. H. Stone
and Lt Mark Jelonek for their support. My thanks and love to
my wife, Beth, who was always supportive and always allowed
me to study when I needed to. Also, my love to Cindy and
Kristin who patiently endured Dad's studies and waited for
tomorrows that rarely came.

Table of Contents

List of Figures

LIST OF TABLES

Abstract

The goal of the experiment was to produce nonlinear optical phase conjugation (NOPC) in fluorescein-doped boric acid glass and in BSO, and to use two-wave mixing (TWM) in BSO to transfer energy between laser beams. Next, the parameters that affect these processes were to be examined. The parameters measured for phase conjugation were the power and intensity of the various beams, angles between the beams, orientation of the BSO crystal, sample thickness and concentration, polarization and wavelength of the incident beams. An Argon Ion and a HeCd laser were used in the experiment. Phase conjugation was produced in BSO at all wavelengths available; 441.6 nm, 457.9 nm, 476.5 nm, 488.0 nm, and 514.5 nm. In fluorescein-doped boric acid, phase conjugation was produced at all wavelengths but 514.5 nm. The maximum diffraction efficiency of shown in fluorescein was higher than in BSO--0.13 % to 0.044 %. The maximum diffraction efficiency in fluorescein was produced at a wavelength of 457.9 nm, at an intensity of 49 mW / cm^2, and a grating spacing of 0.72μm. The maximum diffraction efficiency in BSO was produced at a wavelength of 457.9 nm, at an intensity of 0.2 mW / cm^2, at a β equal to 1, and a grating spacing of 1.06μm. In two-wave mixing experiments the maximum energy transfer was 7.5 % of the weaker beam and occurred when the c-axis was in the plane of the beams and β was equal to 2000.

NONLINEAR OPTICAL PHASE CONJUGATION
IN FLUORESCEIN AND BISMUTH SILICATE (BSO)

I. INTRODUCTION

The surge of interest in the field of nonlinear optical
phase conjugation (NOPC) that began in the 1970's has
continued until today. Much of the interest is due to the
idea of "time reversal," and to demonstrations of aberration
compensation of distorted beams. The use of nonlinear
optical interactions allows many optical information
processing applications to proceed nearly instantaneously.
The interactions are limited only by the response time of
medium and not by the speed of electronic components or the
computing power available to process the information.
Response times of nonlinear media have been demonstrated to
range from picoseconds to seconds (13:158).

NOPC is in the development stage with practical uses yet
to be put into widespread commercial applications. The Air
Force is interested in developing NOPC for many uses
including adaptive optics, lensless imaging, phase conjugate
resonators, image processing, targeting and tracking, and
pattern recognition (7:27, 14:74-83). Currently, work is
being done in many of these areas at Air Force research

1

laboratories, with a goal, in many cases, of developing NOPC for applications in Strategic Defense Initiative (SDI).

In adaptive optics, NOPC may be used to compensate for static and dynamic distortions encountered in optical systems. High power laser systems and atmospheric communication networks are limited by these distortions. By placing phase conjugate mirrors at the ends of the amplifiers used, these distortions can be eliminated.

Lensless imaging would eliminate the difficulties with controlling and adjusting the lenses in optical systems that have large numbers of lenses. NOPC schemes have been proposed to eliminate these alignment problems. Also, methods of removing distortion of three-dimensional images due to propagation through optical fibers have been demonstrated.

A phase conjugate resonator (PCR) is formed when one or both of the mirrors of a laser cavity are replaced with phase conjugate mirrors. This phase conjugate resonator has unique properties which include the ability to compensate for aberrations in the cavity and unconditional stability (13:175, 7:32).

Image processing can be performed by spatially or temporally encoding one or more of the input beams (14:80, 13:156, 7:33). The conjugate beam can be thought of as the algebraic product of the three input fields (as in four-wave

2

mixing). Images have been transmitted "one way" through the atmosphere using this method.

Another area of research has been in developing pattern recognition devices using nonlinear optical phase conjugation. These devices have applications in all-optical associative memories to possibly be used in optical computers. Optical computing offers a distinct advantage in speed of processing over digital computers.

Much research is being directed toward finding materials that will produce NOPC under varying conditions. Over 50 materials have been used to produce NOPC while new materials are still being examined. This thesis will concentrate on two materials; fluorescein, a saturable absorber, and bismuth silicate (BSO), a photorefractive crystal. These materials are similar in that they both have reasonably quick response times ($\sim$1 sec) and can be used with low intensity lasers to produce phase conjugate returns.

The goal of this thesis is to measure and characterize the properties of these materials that affect the production and efficiency of a phase conjugate wave (PCW) generated in both fluorescein-doped boric acid glass and BSO. The parameters that can be measured by using the available equipment include wavelengths, power, angle, and polarizations of the incident beams. Related to NOPC in photorefractive materials is two-wave mixing (TWM) in which energy is transferred from one beam to another. This has

3

possible applications for the amplification of the phase conjugate beam. The parameters that affect TWM are the angle between, the relative power, and the wavelength of the incident beams. Also, the parameters which affect TWM in BSO will be measured.

The thesis will begin in Chapter II by presenting background theory of the processes involved in fluorescein and BSO that produce NOPC. Chapter III will then present the results produced in experimentation and compare them to published results. In Chapter IV, the results will be analyzed and Chapter V will include conclusions and recommendations.

II. THEORY

A. Introduction to Phase Conjugation

Phase conjugation is the process of creating a complex conjugate of an electromagnetic wave and is basically a real-time processing of electromagnetic fields which occurs as a result of nonlinear optical interactions. These interactions couple various input fields to yield the output field. Two important properties of nonlinear optical interactions are relevant to applications using optical phase conjugation. The properties are: the output field amplitude is proportional to the complex conjugate of the amplitude of a given input field and is proportional to the product of one with one or more of the other input fields.

The first property results in an output field, called the phase conjugate wave (PCW) that propagates in a "time reversed" sense relative to the input wave. The medium in which this occurs is then called a phase conjugate mirror (PCM). Monochromatic radiation incident upon such a field will be "reflected" with the output wave propagating as if one were to temporally reverse the wavefront evolution of the incident field as seen in fig. 1. While an ordinary mirror reverses only the normal component of the propagation vector, the PCM reverses both the normal and transverse components.

So, while in an ordinary mirror the angle of incidence is equal to the angle of reflection, a PCM causes the wavefront
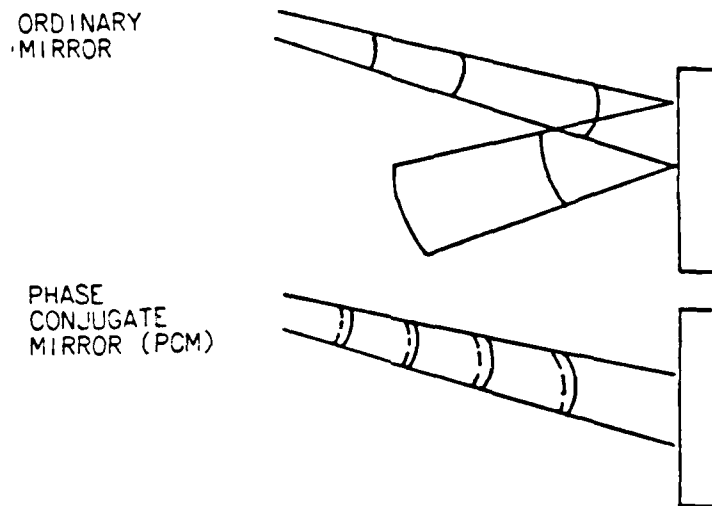
Fig. 1.   Comparison of PCM and Ordinary Mirror

to exactly retrace its path.   This PCW will then "correct" any aberrations in the path of the incident beam as seen in Fig. 2.

Incident   Distorting   PCM
Plane Wave   Medium
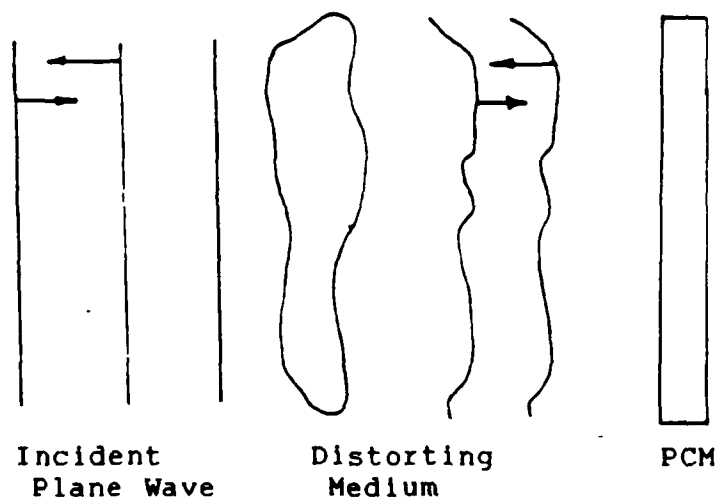
Fig. 2. Aberration Correction Process by Phase Conjugation

The second property relevant to optical phase conjugation is the multiplicative nature of the nonlinear optical interaction. This property is important because of the possible uses of optical phase conjugation in real-time signal processing. By spatially or temporally encoding the various interacting fields, all optical signal processing can be performed.

Entirely different mechanisms produce optical phase conjugation in the two materials used in this experiment, fluorescein and BSO, so the theory will be developed separately. BSO is a photorefractive crystal which means that the index of refraction changes when light strikes it. Other well-known photorefractive materials include $KNbO_3$, $LiNbO_3$, and $BaTiO_3$. Fluorescein produces a phase conjugate wave through a saturated absorption process that changes the state of the fluorescein molecule.

B. NOPC In Photorefractive Materials

The following theoretical analysis will provide some background information about nonlinear optical phase conjugation in photorefractive materials. Nonlinear optical phase conjugation results from the linear electrooptic effect in a medium in response to an electric field. The following wave equation represents an electromagnetic wave propagating in a nonlinear medium.

$$\nabla^2 \vec{E} = \mu_0 \epsilon_0 \frac{\partial^2 \vec{E}}{\partial t^2} + \mu_0 \frac{\partial^2 \vec{P}}{\partial t^2} \qquad (1)$$

where **E** is the electric field, μ_0 is the permeability of free space, ϵ_0 is the dielectric constant, and where P(E) is the nonlinear portion of the polarization vector. P(E) is what allows nonlinear coupling and production of electromagnetic waves in the medium. The polarization depends upon the susceptibility of the medium:

$$\vec{P} = \epsilon_0 \chi (\vec{E}) \vec{E}$$

$$(2)$$

where $\chi(E) = \chi^{(1)} + \chi^{(2)} E + \chi^{(3)} E^2 + \ . \ . \ .$

$\chi^{(1)}$ produces the first order effects such as gain, absorption, dispersion, index of refraction of the medium, and birefringence properties. $\chi^{(2)}$ produces the second order effects such as second harmonic generation and the Pockels' effect. $\chi^{(3)}$ produces third order effects, such as third harmonic generation and phase conjugation, and Kerr effects. The Pockels' effect gives rise to the photorefractive nature of BSO.

Two classes of third order effects are actual Kerr effects and non-local field effects. In the actual Kerr effects, the index of refraction of the material depends upon the field at that point in the crystal. More important in BSO are the non-local field effects. In the non-local field

8

effects, the index of refraction at a point is due to the field at some other point in the medium.

The two classes of non-local field effects include thermal effects and photorefractive effects. In the thermal effects, the intensity pattern produces a temperature gradient across the crystal, causing a spatial modulation of the index of refraction. In the photorefractive effect, the intensity pattern causes charges to migrate, which causes an internal electric field to form. This electric field causes a change in the index of refraction via the Pockels' effect. The charges can migrate due to diffusion or drift in an external field. The dominant mechanism depends upon the crystal type (15:28).

If a photorefractive crystal is then illuminated non-uniformly, a spatial modulation of the index of refraction can be created. Charge donors in the material are needed for this to occur. The charge that migrates can be negative or positive and is typically provided by crystal lattice defects or other materials that have been doped into the crystal. The density of these defects or impurities is an important factor in the speed and efficiency of phase conjugation in these materials. Upon absorption of a photon of sufficient energy to ionize the charge, the charge is free to move until trapped at some other point in the crystal. This process will continue until the charge is trapped in a dark area of the crystal (4:1301).

Efficient charge migration is an important factor in photorefractivity since the rate of migration largely determines the response time of the medium to an applied field. The rate of migration is affected by temperature, direction and magnitude of the applied field and upon the type of crystal and impurity composition (15:28).

The photorefractive effect can then be used to set up a photorefractive grating or index grating in the medium. The photorefractive grating can be formed by the intersection of two coherent beams of light which set up a three-dimensional interference pattern. Charge will then migrate from light to dark areas creating a modulation of the index of refraction. However, the maximum change of the index of refraction occurs where the maxima in the electric field are, so the maximum change in the index of refraction is shifted by a quarter of the period of the intensity pattern as seen in Fig. 3. This is the origin of the non-local response of the medium (9:30). The phase shift between the intensity maximum and the maximum change in index of refraction enables the transfer of power from one beam to another via two-beam coupling.
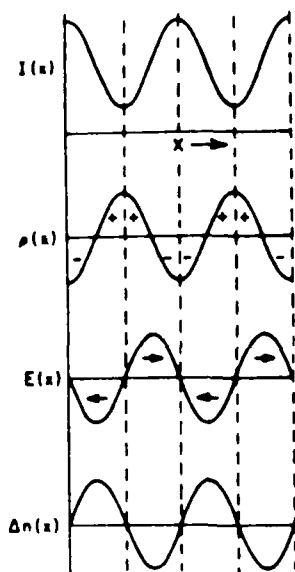
Fig. 3.   Diagram of Intensity and Index Maximum

C. Phase Conjugation and Two-Beam Coupling in BSO

BSO is a photorefractive crystal in which two-wave
mixing (TWM) and degenerate four-wave mixing (DFWM) can
easily be demonstrated. Some advantages of this material are
its large nonlinearity which makes it possible to achieve
phase conjugation with low power laser beams; low dark
conductivity; large, high quality crystals which can be
grown; and it demonstrates quick response times. However,
the phase conjugation does not exhibit high efficiency
(~ 0.1 %).

In BSO, phase conjugation and TWM are achieved using the
index grating which is formed by the movement of charges as
discussed in the last section. Two mechanisms by which the

11

charges move are diffusion and drift in an external field. Diffusion is a process of migration that occurs because of the light and dark areas of the crystal as described earlier. The diffusion process can be enhanced by applying a voltage across the crystal which adds drift to the migration process, increasing the distance traveled before the charge is trapped at some later point. For BSO, the two processes contribute equally to the migration process when the electric field applied is equal to 2 kV / cm (10:102). At field strengths larger than this, the drift mechanism dominates. Because of the technical complexity involved in applying a voltage across the crystal, no voltage was applied in this experiment.

BSO is an electrooptic, photoconductive crystal with a cubic point group symmetry, ($\bar{4}$3m), so it is optically isotropic. When an electric field is applied the crystal becomes birefringent because of the non-vanishing Pockels' coefficient (8:240). BSO is strongly optically active with a rotation of 40 degrees / mm at 514.5 nm according to Abrams (2:293) or 45 degrees / mm according to Gunther (8:240). Table I below shows the rotation for various wavelengths as taken from Abrams (2:293). Other parameters of BSO are shown in Table II.

The orientation of the c-axis of the crystal with respect to the incident beams determines whether the crystal will produce maximum diffraction efficiency (η) through DFWM

or maximum energy transfer via TWM as seen in Fig. 4.
Since η is approximately equal to (Δn), it can be seen that η
is larger for the orientation in b.) of Fig. 4.

Table I. Optical Activity in BSO
(2:293)

Wavelength (nm)	Rotation (degrees/mm)
420	80
450	60.2
500	42.2
550	31.6

Table II. BSO Material Parameters

Absorption Coefficient (α)	1.3 - 3.0 cm	(8:215)
Dark Conductivity (σ_d)	10^{-5} ohms/cm	(8:215)
Index of Refraction (n)	2.540	(8:215)
Electrooptic Tensor Elements (r63 = r41 = r52)	5 pm / v	(8:427)
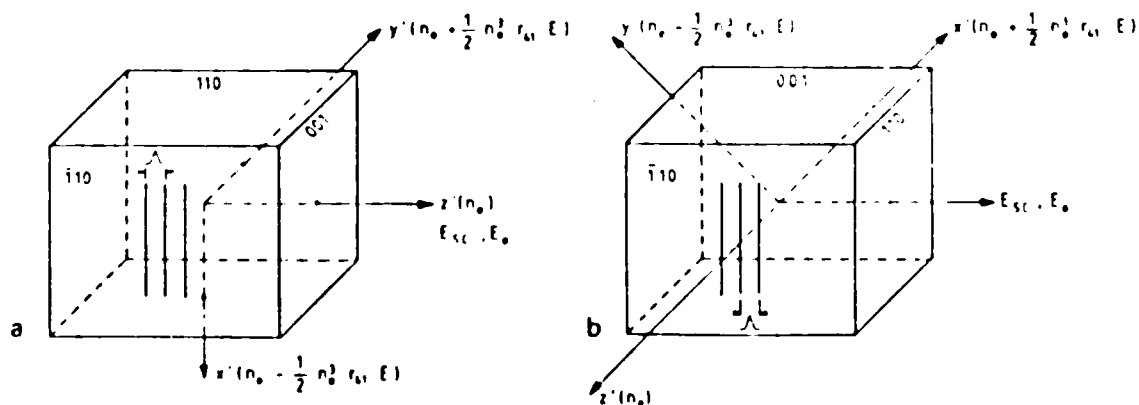
a.) (Δn) = (1/2) $n^3 r_{41}$ E   b.) (Δn) = $n^3 r_{41}$ E

Fig. 4. Crystal Orientation for a) Maximum Energy
Transfer or b) Maximum Diffraction Efficiency (or
Reflectivity)

(8:241)

13

The geometry of DFWM is shown in Fig. 5. Several gratings are formed in the medium, both reflection gratings and transmission gratings (8:241). Beams R1 and S3 write a transmission grating that diffracts R2. The diffraction of R1, by a reflection grating formed by R2 and S3, produces additional phase conjugate wave S4 .
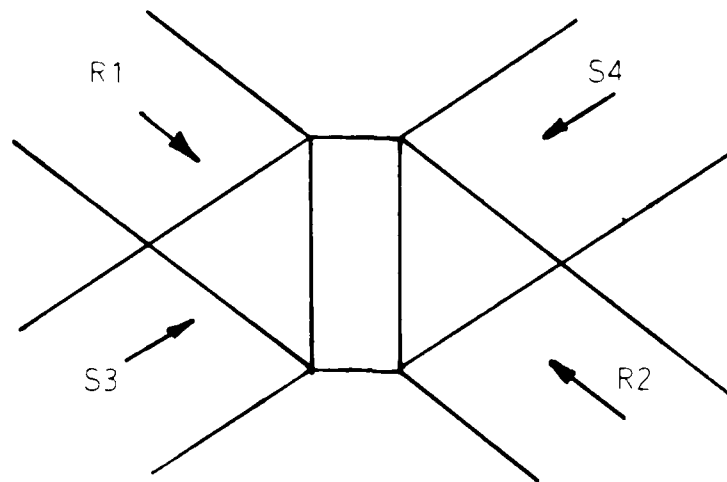
Fig. 5. Four-Wave Mixing Geometry

In TWM, just R1 and S3 would be incident to the BSO, with energy transfer to either beam as it exits.

As stated earlier, the space-charge field in BSO is set up by diffusion due to the incident radiation and drift due to the external field if a voltage is applied transversely. In the experimental section to follow, no voltage will be applied. So, neglecting drift, the reflectivity, ρ (S4/S3), of DFWM in BSO is given by (8:257, 10:103).

14

$$p = \frac{4\beta \, (\delta \, d \, F \, E_d)^2 \, \exp(-2\alpha d)}{[\, 1 + \beta \exp(-\alpha d)\,] \, [\, 1 + E_d / Eq\,]^2} \qquad (3)$$

where

$$\delta = \frac{\pi \, n^3 \, r}{\lambda \, \cos \theta} \qquad (4)$$

θ is the angle between the beams, n is the refractive index of the crystal, r is the selected electrooptic coefficient, d is the length of the crystal, E_d is the diffusion field, Eq is the space charge field, α is the absorption coefficient and β is the ratio of the intensities of S3 to R1 and F = 1 or 0.5 depending upon the charge recombination mechanism.

The factors that can be varied for a given crystal are θ, β, λ, E_d and Eq. E_d is given by

$$E_d = \Lambda^{-1} \, kT / e \qquad (5)$$

where Λ is the fringe spacing (which is dependent upon θ), k is Boltzman's constant, T is the temperature of the crystal and e is the electronic charge. Eq is given by

$$Eq = 2 \, e \, N \, \Lambda / \epsilon_0 \epsilon_r \qquad (6)$$

where ϵ_0 is the permittivity of free space, ϵ_r is the relative

15

permittivity, and N is the concentration of trapping centers in the crystal. These are the factors for a given crystal that can be changed to affect the reflectivity as well as the diffraction efficiency, η. Although diffraction can take place in both geometries in Fig. 4, the geometry of b.) is four times as efficient, theoretically. Experimentally, Gunter gives the following results under these conditions (8:260); I = 16 mW / cm^2, Λ = 1.1 microns, and d = 10 mm. γ is the gain of the signal beam, S3 (intensity of output beam with second beam present divided by the intensity of the output beam with the second beam removed). η is the ratio of S4 to R2.

      a.) Maximum energy transfer configuration.

$$\beta = 1 \qquad \eta = 0.21 \%$$

$$\beta = .008 \qquad \gamma = 1.3$$

      b.) Maximum efficiency configuration.

$$\beta = 1 \qquad \eta = .68 \%$$

$$\beta = .008 \qquad \gamma = 0;\ \text{no beam coupling}$$

In addition, Gunter states,

> . . . the direction of the energy transfer
> in BSO depends on the sign of the grating shift
> [direction of index grating shift with respect to
> the intensity grating] which in turn is connected
> with the z'-axis [of the index ellipsiod]. In
> the appropriate configuration, the intensity may
> be transferred from the weak to the strong beam
> (8:261).

Also, the sign of the mobile charge carriers can be determined by the direction of the energy transfer with respect to the c axis of the crystal (5:431). For an isotropic crystal such as BSO, however, a preferred direction of energy transfer seems unlikely since the crystal is isotropic with the +c and -c axes identical. This will be investigated in the experiment to follow. Fig. 6 shows the energy transfer in barium titanate which has positive mobile charge carriers but is not isotropic.

Diffraction efficiency and energy transfer are also dependent upon incident beam intensity and B, which is the ratio of incident beam intensities. Diffraction efficiency saturates due to the trap filling mechanism. When acceptor levels are completely filled with the incident photo-generated electrons, the BSO diffraction efficiency saturates, meaning that higher intensities will not increase diffraction efficiency.
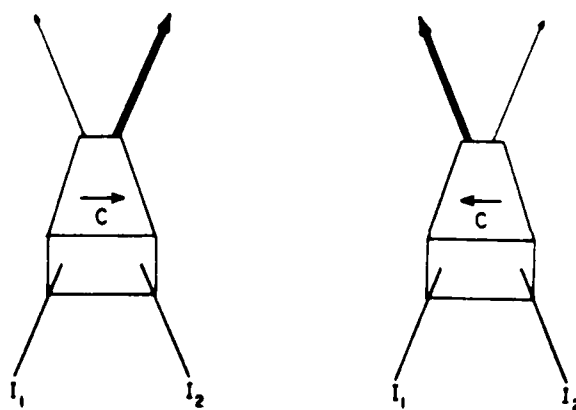
Fig. 6. Energy Transfer in Barium Titanate
(4:1301)

Energy transfer saturates at about 30 times lower intensity than diffraction efficiency. Energy transfer saturates at $\beta = 100$ and diffraction efficiency peaks at $\beta = 1$ (8:265).

D. NOPC in Fluorescein-Doped Boric Acid Glass

Another method of producing NOPC is through the use of saturable absorbers. Large nonlinear susceptibilities resulting from the nonlinear response of the molecules have been demonstrated (12:2026, 16:265, 17:209, 6:386). The saturable absorbers used have been in several different forms; in liquid solution, single crystals of the material, and doped into various solids. Advantages of these materials are the low intensity of light that is required to that is required to produce phase conjugation, and the speed at which phase conjugation occurs.

The mechanism used in typical saturable absorber to generate the phase conjugate wave (PCW) involves the excitation of the molecule in the ground singlet state to the excited singlet state. The molecules then transition back to the ground singlet state. A small percentage of the molecules, however, transition into the lowest energy triplet state which acts as a trap with a finite lifetime as seen in Fig. 7. This is known as an intersystem crossing (16:266).

18
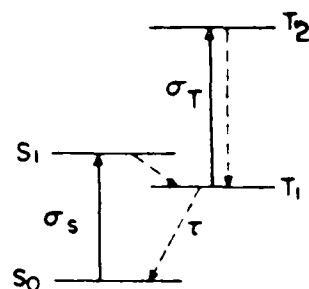
Fig. 7.   Energy Level Diagram for a Four-Level Saturable
Absorber (where σ_s is the cross section absorption
for $S_0 - S_1$, σ_t is the cross section absorption
for $T_0 - T_1$, and τ is the lifetime)

The triplet state then exhibits a changed index of refraction

which in turn is used to form the index grating. The

lifetime of this triplet state depends upon various quenching

mechanisms, more of which occur in liquid form than in solid.

Typically, in solid form, the only decay mechanism is

thermally-activated delayed fluorescence (12:2027). In

liquid dye solution oxygen that exists in the solution is a

very efficient quenching mechanism, and, therefore, decreases

the lifetime by several orders of magnitude (16:267), which

in turn, raises the saturation intensity accordingly. In

solid form, i.e. a glassy solid; however, the effects of

oxygen are negligible (16:267).

Also in liquid form, there tends to be a smearing of the

grating formed which lessens the desired intensity grating

and degrades the resolution of the diffracted beam. Maximum efficiency is obtained when the saturable absorber is in a solid form. This can be seen in the equation for saturation intensity given by Kramer (12:2026).

$$I_s = \hbar\omega / \sigma_s T \qquad (6)$$

where Is is the saturation intensity, σ_s is the cross section absorption of the ground singlet state, and T is the lifetime in the lowest triplet state. The susceptibility χ of the medium is dependent upon the saturation intensity though (1:95)

$$\chi(E) = \frac{-2\alpha_o(1+\delta)}{k[1+\delta^2 + |E/Es|^2]} \qquad (7)$$

where δ is the normalized detuning from linecenter, α is the absorption coefficient, k is the magnitude of the wavenumber at frequency ω, and Is, the saturation intensity is equal to the magnitude squared of Es ,the saturation electric field. Equation (7) is applicable when the molecules are in solid form and the electric fields are polarized in the same direction. This equation can then be related to equations (1) and (2) through χ and the polarization.

Fluorescein is a saturable absorber, organic laser dye which has useful properties for low-intensity phase conjugation via degenerate four-wave mixing (DFWM). When it

20

is held rigidly in a glassy material, the lifetime of the lowest lying triplet state is .1 to 1 second (12:2027), σ_s, as seen in Fig 7. has a value of $1.5 \times 10^{-16} cm^2$ at 457.9 nm, and σ_t has a value of $3.0 \times 10^{-16} cm^2$. 0.1 second taken as the value of the lifetime, gives a saturation intensity at linecenter of approximately 15 mW / cm^2 according to equation (6). While the reflectivity of the material is low, generally no more than 0.6 percent (12:2026), the ability to produce a PCW at such low intensities makes this material worthy of further investigation.

Several methods of preparing fluorescein in a rigid film have been discussed in the literature, with the most common method being doping the fluorescein into a boric acid glass. Typically, a .01 to .001 M solution of Fluorescein in boric acid is pressed to a thickness of 100 to 200 μm between two glass slides. Samples thicker than this have a tendency to crack severely upon cooling.

The wavelengths that will produce the grating in the fluorescein must be close enough to the absorption linecenter of fluorescein to produce sufficient triplet state population in the medium. The absorption peak is at 440 nm for fluorescein-doped boric acid glass (8:2027) so the lines of an argon ion laser at 457.9, 476.5, 488.0 and 514.5 nm should produce the desired effects. Also, a HeCd laser will be used which produces a line at 441.6 nm.

21

As in BSO, the diffraction efficiency of the fluorescein-doped boric acid glass depends upon several factors and, for a given sample, some are controllable and some are not. Bar-Joseph (3:455) gives the diffraction efficiency as

$$\eta = \exp [- 2 \alpha_{0t} / \cos \theta] \sinh^2 [\alpha_{1t} d / \cos \theta] \quad (8)$$

where α_{0t} and α_{1t} are the bias term and modulation term of the absorption coefficient of the lowest-lying triplet state. α_{0t} and α_{1t} are the first two coefficients in the Fourier expansion of α_t, which is equal to the cross section term σ_t
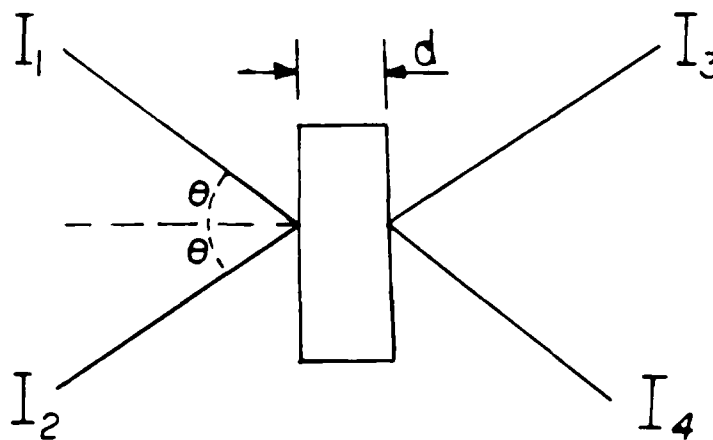

Fig. 8. Geometry for DFWM in Fluorescein-Doped Boric Acid Glass

22

multiplied by n_t, the population of the triplet state as a function of incident intensities. The thickness of the nonlinear medium is d and θ is the angle between the beams and is shown in Fig. 8.

α_{0t} and α_{1t} are given by

$$\alpha_{0t} = n_0 \sigma_t \times \left[\frac{(1-P)^{1/2} - Is / (I_1 + I_2 + Is)}{(1-P)^{1/2}} \right] \quad (9)$$

$$\alpha_{1t} = n_0 \sigma_t \times \frac{Is[1 - (1 - P)^{1/2}]}{[2 (I_1 I_2)^{1/2}(1 - P)^{1/2}]} \quad (10)$$

where $P = (4 I_1 I_2) / (I_1 + I_2 + Is)$, where n_0 is the density of molecules in the fluorescein-doped boric acid glass, and Is is the saturation intensity.

So for fluorescein-doped boric acid glass in equations (8), (9), and (10), the terms which are not controllable for a given sample are n , d, σ_t, and Is. However, all terms but are controllable if the making of the sample is included.

According to Bar Joseph, the diffraction grating exhibits a transient nature which is characterized by an overshoot of the steady state value of n when the intensities of the incident beams are much higher than the saturation intensity of the sample (3:456). The transient nature of the PCW is due to the population of the molecules in the triplet state forming the diffraction grating. When intensity of the writing beams is much larger than the saturation intensity, the grating is transformed from a sinusoidal grating to a distorted grating (3:457).

23

III. EXPERIMENT

A. OVERVIEW

The goal of this experiment was to produce nonlinear optical phase conjugation in fluorescein-doped boric acid glass and BSO, and to demonstrate two-wave mixing (TWM) in BSO. The parameters that affect the production of a PCW and the parameters that affect energy transfer in TWM were then to be measured. The parameters to be measured for the phase conjugation include power and intensity of the various beams, angles between the beams, orientation of the BSO crystal or sample concentration and thickness, polarization of the incident beams in both cases, and wavelengths of the incident beams. The effect of these parameters upon the speed, efficiency, and reflectivity of the PCW will then be analyzed. The parameters to be analyzed in TWM are angle between the beams, orientation of the crystal, relative power of the beams and wavelengths of the incident beams.

Initially, work was begun in fluorescein-doped boric acid glass. The samples supplied by Kramer at the Air Force Weapons Lab were of unknown concentration, so samples of known concentration were later prepared in the lab to better quantify results. About midway through the research period, a BSO sample became available so research was done using both materials.

24

The experimental section will be divided into three sections, fluorescein-doped boric acid glass NOPC, BSO NOPC and BSO TWM. The equipment used in the experiment will be discussed as needed.

B. NOPC in Fluorescein

The fluorescein-doped boric acid glass samples obtained from Kramer were used in the setup shown in fig. 9 to generate phase conjugation. The angle between the probe and write beams was approximately five degrees.

A Spectra Physics Model 162-07 Argon ion laser was used as a source. The maximum output of this laser varied with wavelength as seen in Table III.

Table III. Maximum Wavelength Output Power for Wavelengths of Argon Ion Laser

Wavelength (nm)	Maximum Power Output (mW)
457.9	4
476.5	8
488.0	26
514.5	27

The low power at 457.9 nm proved to be a disadvantage for NOPC in fluorescein since the lowest power line is the one that is closest to the absorption peak of the fluorescein. The efficiency was later found to be the

highest at this wavelength, but the input power was so low as
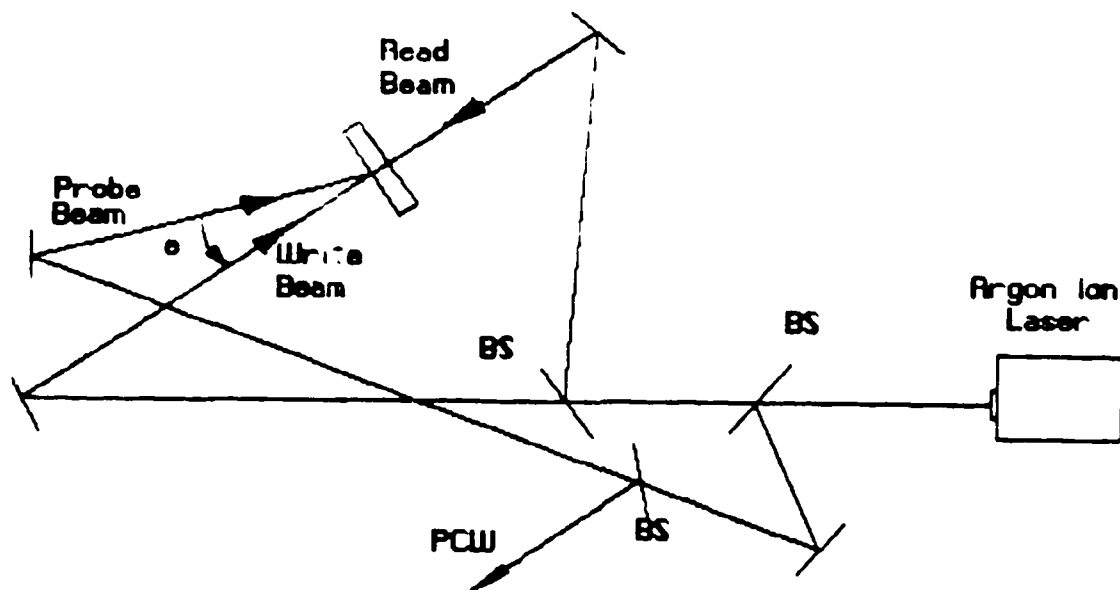to limit the PCW power.

Fig. 9. Setup for Phase Conjugation in Fluorescein-Doped
Boric Acid Glass

Several factors need to be considered when attempting to
produce phase conjugation. The beams that write the grating
must be coherent with each other, so the path length
difference in the two beams must be less than the coherence
length of the laser. Also, vibration in the setup must be
held to a minimum. The phase grating takes a finite time to
write, so vibrations will tend to wash out the grating before
it can form, eliminating any possible PCW generation.
Another consideration in fluorescein is the angle between the

26

writing beams. The smaller the angle, the greater the spacing between the fringes. The larger spacing will help to counteract the effect of vibrations. The wavelength, also must be near enough to the absorption peak of the fluorescein to benefit from the resonant enhancement of the susceptibility.

With all of this in mind, the coherence length of the laser was measured with a Michelson interferometer made of a beam-splitter and two mirrors. Fringes were visible out to a 1.2 meter path difference; however, the visibility was greatly diminished at large path length differences. Assuming coherence length of greater than 1.2 m turned out to be a costly error as three weeks went by before steady phase conjugation was produced because of too large a path length difference. A wavelength of 457.9 nm was used, the angle between the pump and probe beams was set at 5 degrees and the path length difference was about 24 cm.

The pump (write) and probe beams then were made equal in intensity to increase the grating efficiency. Also, as a test for grating formation, a HeNe laser beam was directed to the grating region of the sample. The HeNe was set up as in Fig. 10.

When the setup in Fig. 9, with the 457.9 line of the argon with equal intensity pump and probe beam, was used, the HeNe was diffracted as shown in Fig. 10. It was then a simple matter to produce NOPC using the setup from Fig. 10.

27

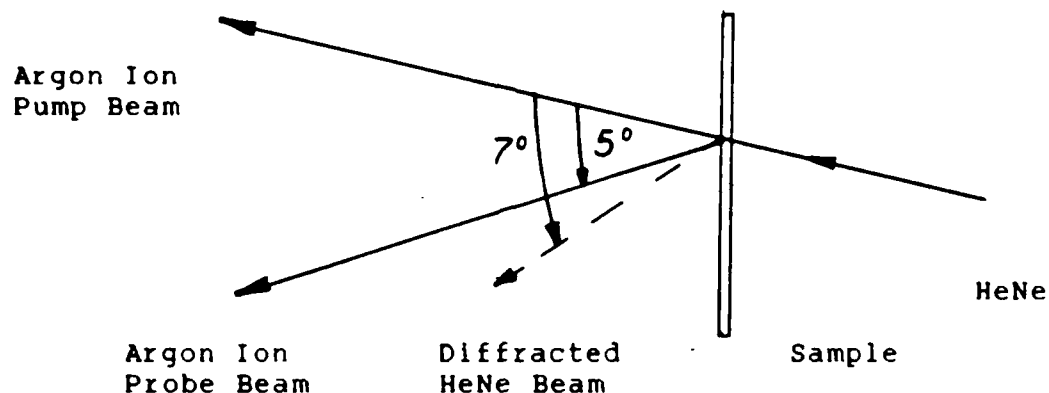However, during an adjustment, the phase conjugate beam disappeared.

Fig. 10. Geometry for HeNe Diffraction in Fluorescein

After two weeks of trying to duplicate these results, the coherence length of the laser was rechecked and it was observed that at 7 cm path length difference, the visibility of the fringes was greatly reduced to nearly indistinguishable levels, similar to what appeared at 1.2 meters path length difference earlier. It was then determined that the "good" coherence length was only 7 cm. Once the coherence length was found to be smaller, the phase conjugation experiments were much easier to perform

Two samples of different thicknesses of fluorescein-doped boric acid glass were available as supplied by Kramer.

28

The thicknesses were approximately 100 and 300 microns. The
thicker sample produced a much higher efficiency than the
other; however, the sample was cracked before the experiment
started and soon was unusable.

Additional samples of fluorescein-doped boric acid glass
were then made to provide thicker, usable samples. The
process for making the fluorescein-doped boric acid glass is
described in literature and the process is fairly simple
(12:2026, 17:209). To make a .001 M solution of fluorescein
in boric acid, the following calculation was made using the
gram molecular weight of fluorescein, 412 g/mole, and the
density of boric acid, 1.439 g/cc.

$$\frac{\dfrac{412g\ fl.}{mole} \times .001\ mole\ fl.}{\dfrac{1,439g\ B.\ Acid}{cc} \times 1000\ cc\ B.\ Acid} = \frac{.412gfl.}{1435g\ B.\ Acid} \quad (11)$$

This provided the ratio of fluorescein to boric acid to
provide a .001 M solution of fluorescein. The amounts then
measured to mix were 20.6 mg fluorescein and 71.750 g boric
acid. This would have made a .001 M solution of fluorescein.
Eventually, only 46.7442 g of boric acid were used, making
the solution a .00154 M solution.

The process was as follows: all the fluorescein was
placed in test tube and a small amount of the boric acid was
added until the test tube was one-quarter filled. This
mixture was slowly heated with a Bunsen burner until it
became a yellow liquid. The boric acid was then added slowly

29

while the heating process continued. The boric acid condensed greatly as it melted. Because of the large amount of boric acid to be added, this was a long, tedious effort. Eventually, it was decided that if all of the boric acid was included, the test tube would be too full for safety and accuracy, so only 46.7442 g of the boric acid were used. Microscope slides were cleaned with methanol and placed on hot plate next to the Bunsen burner. These must be heated to allow the mixture to cool slowly enough to let it spread and yet not so hot that the mixture bubbles when placed upon the slide.

Small amounts of the heated mixture were then dipped out onto the slides and then pressed with a second heated slide. The temperatures of the hot plate was then slowly lessened until cool. Once cooled, many of the samples produced severe cracking. These samples were then reheated and then pressed to form a thinner layer and recooled.

Eventually, 10 usable samples were produced, ranging in thickness from 50 to 426 microns, with the thicker samples being somewhat cracked but usable. With the amount of the mixture that was left over, 500 samples probably could have been made, so much less fluorescein and boric acid could have been used.

The samples were tested and were found to produce excellent NOPC results with efficiencies approaching 0.1 percent at 457.9 nm. A He-Cd laser was used in place of

30

the argon ion laser to produce additional data points. This
laser produced 9 mW of power at 441.6 nm. This wavelength is
centered (within 2 nm) on the absorption curve of
fluorescein. It was thought that this wavelength component
would be absorbed too much to allow the efficient production
of the phase conjugate wave. The highest measured was .05
percent which was lower than the results of Argon at 457.9
nm.

Since aberration compensation is one of the more
promising properties of NOPC, this was the first test done on
the phase conjugate return. The photograph in Fig. 11 a.)
shows the phase conjugate beam before the system contained an
aberrating medium.

When an aberrating medium is placed in the path of the
probe, care must be taken to collect the light scattered by
the aberrating medium to provide enough photons incident upon
the fluorescein to produce a phase conjugate return. A lens
placed after the aberrator served well to collect the light.

Fig. 11 b.) shows the aberrated beam due to a glass
slide etched with hydrofluoric acid placed in the path of the
beam. The PCM was replaced with a normal mirror to show the
uncorrected beam. Fig. 11 c.) then shows the corrected beam
with the aberrating medium still in the beam. The power in
c.), however, was much less than the power in a.) due to
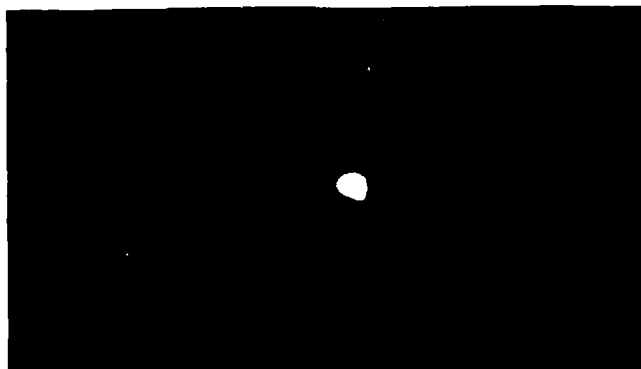loses caused by the scattering of the beam by the aberrator.

31
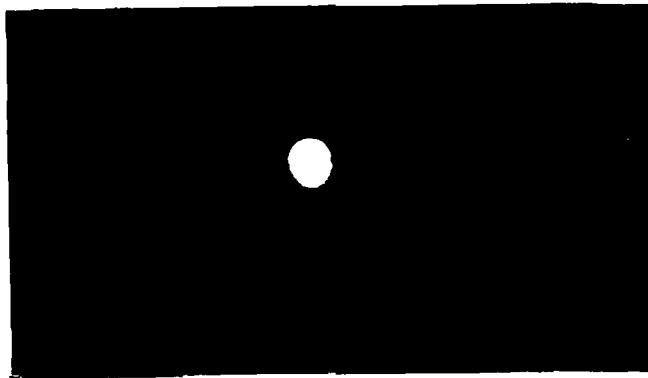
Fig. 11. Photographs of Aberration Compensation in
Fluorescein-Doped Boric Acid Glass (a.) unaberrated beam,
b.) aberrated beam with PCM replaced with ordinary mirror,
c.) PCM compensated)

32

The efficiency of the process was highest for 457.9 nm (although this line had the lowest maximum power of the Argon lines) and decreased as wavelength increased. At 514.5 nm, no phase conjugation was detected. The highest efficiency obtained was 0.14 percent at 457.9 nm, 37 degrees between the beams 0.5 mW pump beam power, 0.3 mW read beam power and .2 mW probe beam power. The beam diameter at the sample was 2 mm, so the beam intensity of the write beam was 15.9 mW / cm^2, which approached the saturation intensity of fluorescein at this wavelength of 30 mW / cm^2 where the efficiency should be maximum. The efficiencies for different wavelengths versus intensity are also shown in Fig. 12.
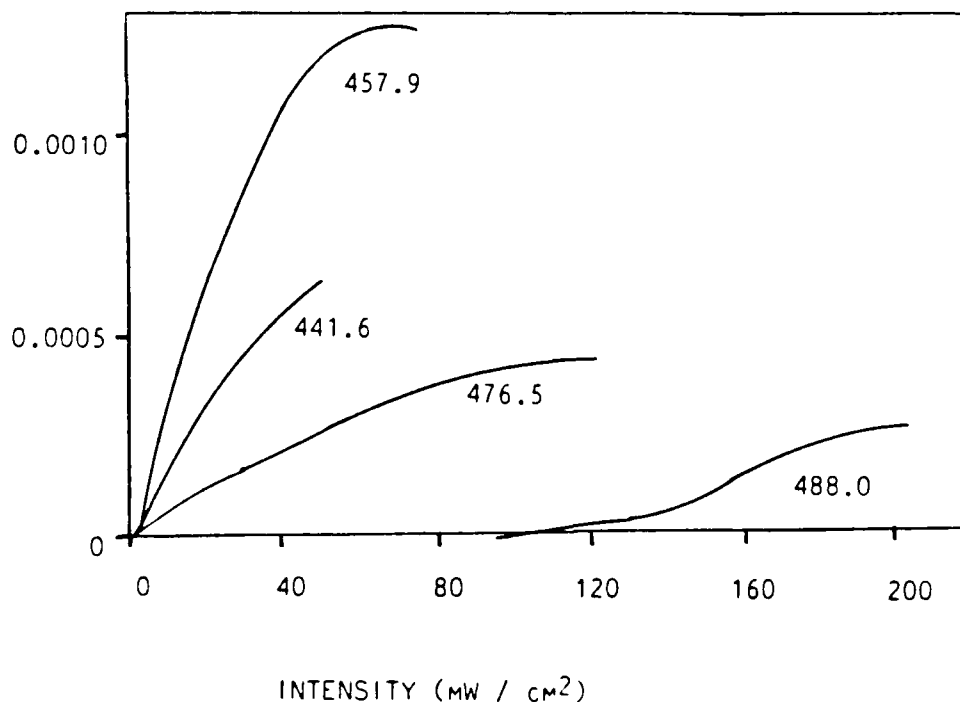

Fig. 12.   Diffraction Efficiency for Various Wavelengths in Fluorescein

From the results above, it is clear that the wavelength used must be close enough to the line center of the absorption curve to allow resonant enhancement of the nonlinear susceptibility, but must be detuned enough to avoid large absorption losses. The thickness of the sample also played a role in determining the diffraction efficiency. As seen in Fig. 13, the increasing of the sample thickness increases the efficiency dramatically.
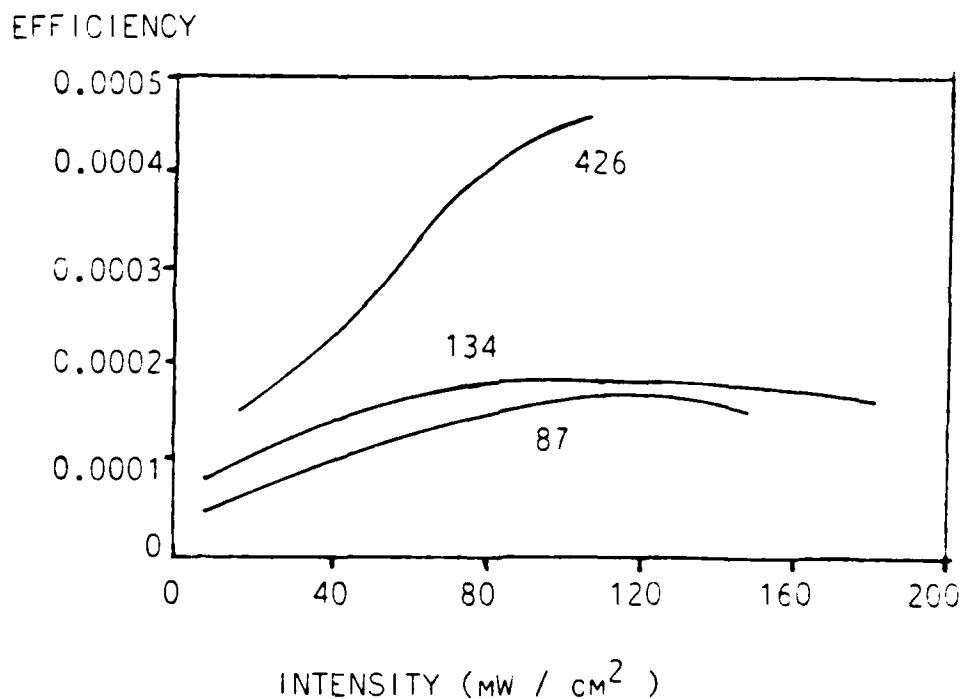
EFFICIENCY

INTENSITY (MW / CM^2)

Fig. 13. Diffraction Efficiency as a Function of Intensity for Varied Sample Lengths (Θ = 37°, β = 0.37, λ= 488.0 nm)

Although the angle dependency was difficult to measure, the samples produced maximum efficiency near 40 degrees (between write and probe beams). The grating spacing for

this angle is .7 to .8 microns. This does not agree totally with Kramer's statement that for gratings less than 1 micron the efficiency was nearly zero (12:2027).

The intensity of the PCW is shown in Fig. 14 for various input intensities. As noted earlier, an overshoot of the steady state value should occur when the intensity is higher than saturation intensity at that wavelength, which is shown in Fig. 14 for the two higher intensity lines. Also, the PCW is less stable at higher intensities. The mechanical vibrations, evidently, have a larger effect upon the PCW, at higher output levels.
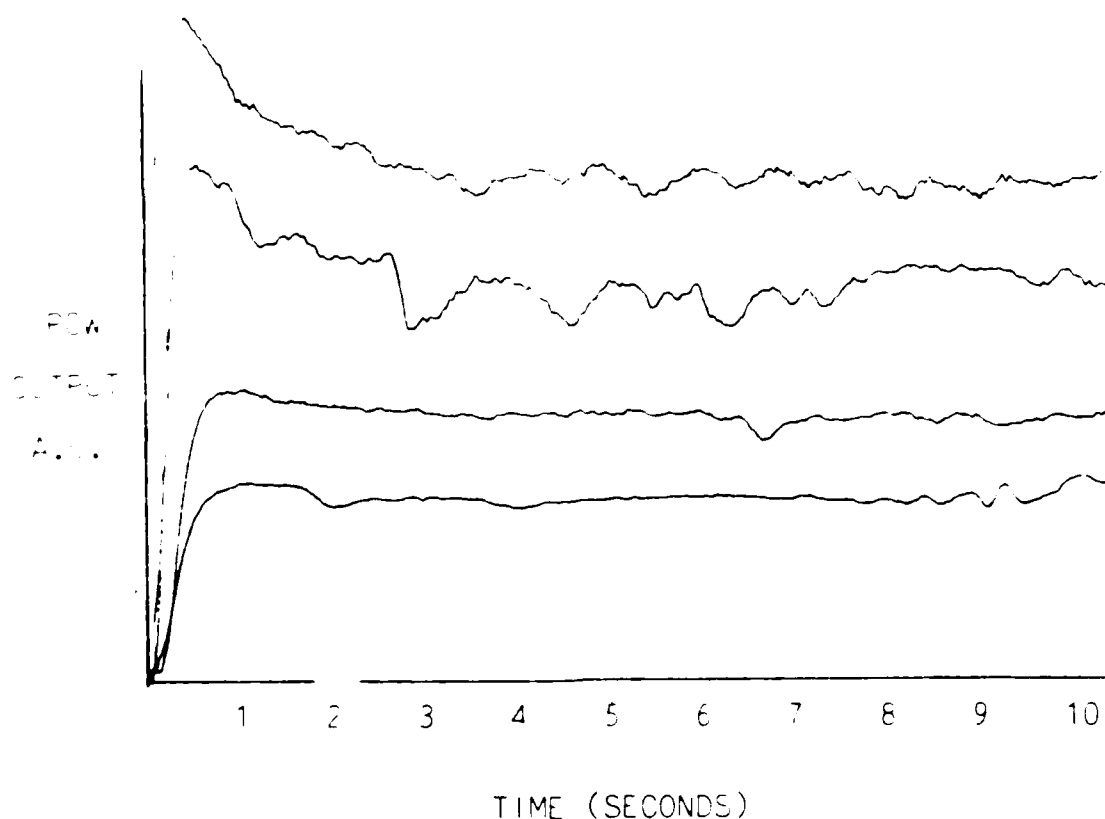

TIME (SECONDS)

Fig. 14.   Fluorescein PCW for Various Intensities
at 457.9 nm

35

The 0 to 100 % rise time of the phase conjugate wave is shown in Fig. 15 as a function of both intensity and wavelength. The shortest rise time was 0.1 seconds using a 457.9 nm wavelength at 9 mW / cm^2. The rise time increases as the wavelength used gets farther from the absorption linecenter of fluorescein at 440 nm. Due to the laser used, the maximum intensity producible at 457.9 nm was 9 mW / cm^2 so the curve for 457.9 nm ends before the shortest rise time could be found.
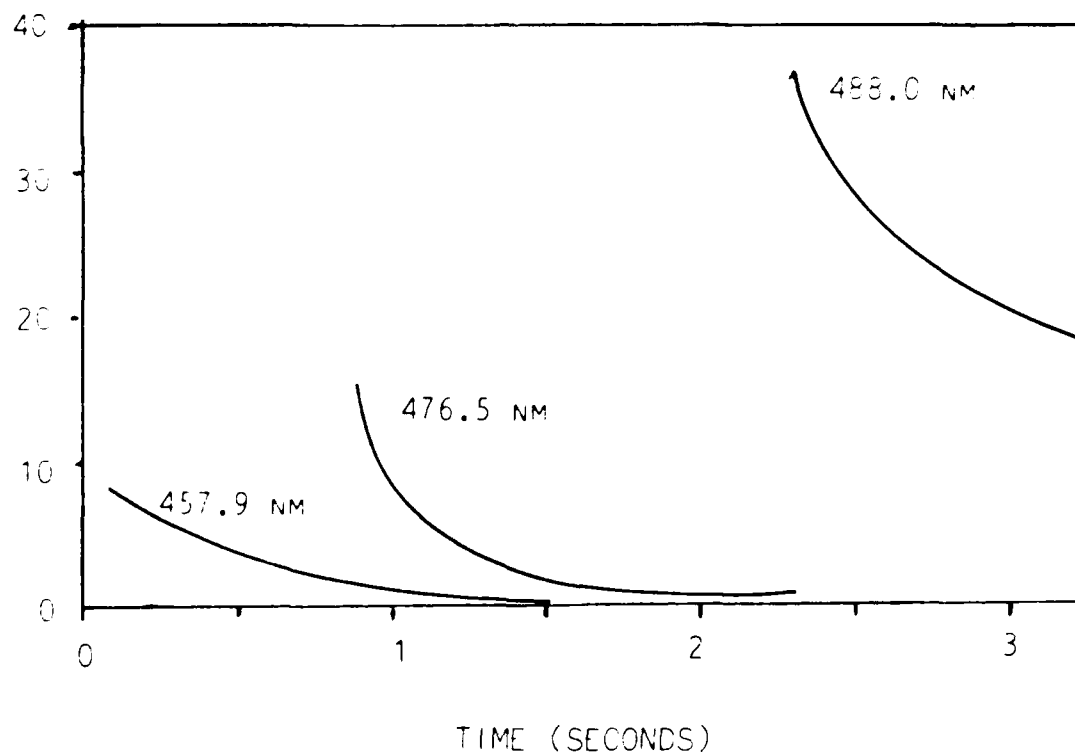
INTENSITY

MW / CM^2

Fig. 15. Rise Time of PCW in Fluorescein for
Various Wavelengths

C. BSO NOPC Experimental Results and Analysis

The experimental setup for NOPC using BSO is pictured in Fig. 16, where the three incident beams are propagating in the XY plane (if the c-axis is Z). The read beam, which is counterpropagating to the write beam, is generated by reflecting the write beam back onto itself. The c-axis is
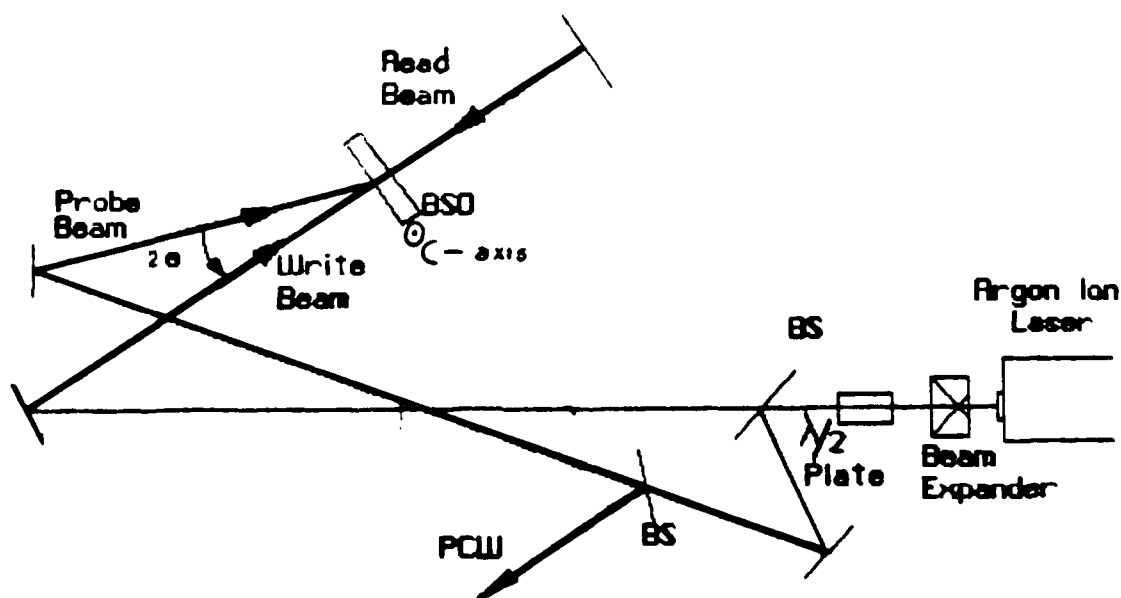

Fig. 16. Experimental Setup for NOPC in BSO

perpendicular to the plane of the figure so this is the configuration for maximum diffraction efficiency (see Fig. 4). From various sources, the optimum angle given

37

for NOPC in BSO with no transverse voltage applied is one
that will make the grating spacing slightly less than one
micron. Fig. 17 shows the relationship between θ and grating
spacing.

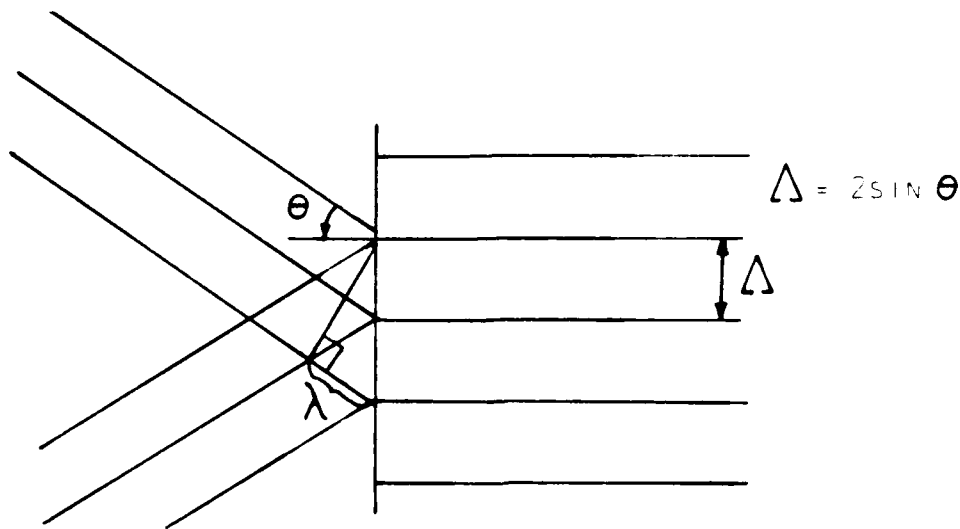$$\Lambda = \frac{\lambda}{2 \sin \theta}$$

Fig. 17. Grating Spacing in BSO

So 2θ was set at approximately 29 degrees for the
initial attempts to produce phase conjugation which produced
a grating spacing of 0.97 um at 488.0 nm. The beam expander
was used so the size of the beam at the BSO crystal could be
controlled. The half-wave plate was used to adjust the
polarization of the output of the laser to the desired angle.
The detector was a silicon detector which was sensitive down
to thousandths of $\mu W / cm^2$. Since typically the beam
diameters were on the order of two to four mm and the
detector was 1 cm^2, all power of a beam could be directed
into the detector. Since the detector was calibrated in $\mu W /$

38

cm^2, power was read directly from the meter. The polarization of all beams was vertical initially.

The phase conjugate was produced as expected. The efficiencies produced were in the 1×10^{-4} range as predicted in the literature. The BSO crystal did exhibit maximum diffraction efficiency with the c-axis normal to the plane containing the incident beams. When the c-axis was rotated to lie in the incident plane, the output dropped at least to less than one half of the previous output. Now several parameters could be tested, such as effects of various polarizations, efficiency as it related to angle between the beams, intensity in the beams, ratios of intensity in the beams and rise times of the phase conjugate return for various intensities and wavelengths.

The first parameters to be measured were the effects of polarization upon the phase conjugation and the polarization of the phase conjugate waves. A quarter-wave plate was inserted in the read beam in Fig. 16, so upon two passes through it, the quarter-wave plate acted as a half-wave plate and the polarization could be controlled before it reentered the BSO. Also, a Glan prism was inserted before the detector so the polarization of the phase conjugate wave could be determined. This was based upon Feinburg's statement that horizontal polarization would return as vertical and vertical polarization would return as horizontal (4:427). However, after testing for all possible combinations of polarizations,

39

the PCW always seemed to favor the vertical polarization. At first, this was assumed to be a problem of polarization-dependent transmission and reflection at the beam splitter in front of the detector. A characterization of the beam splitter was made for horizontal and vertical polarizations for all incident angles and the information was used to "correct" the values found. Still, no real pattern could be found that matched Feinburg's prediction.

Feinburg had stated several lines before the statement on polarization that he was ignoring optical activity, so it was assumed by this researcher to be negligible. However, BSO is strongly optically active and the phase conjugate return is elliptically polarized. The measured optical activity of BSO at several wavelengths is shown in Table IV. The measured values agreed closely to the values in Table I. The laser was directed through the crystal and the output polarization was measured. The optical activity stayed

Table IV. Measured Optical Activity In BSO

Wavelength (nm)	Rotation of Polarization Degrees/mm
514.5	38.75
488.0	45.00
476.5	47.50
457.9	53.25

constant for a given wavelength for any input polarization.
The crystal was four mm thick. Fig. 18 compares these values
to the values measured by Abrams (2:293).

WAVELENGTH
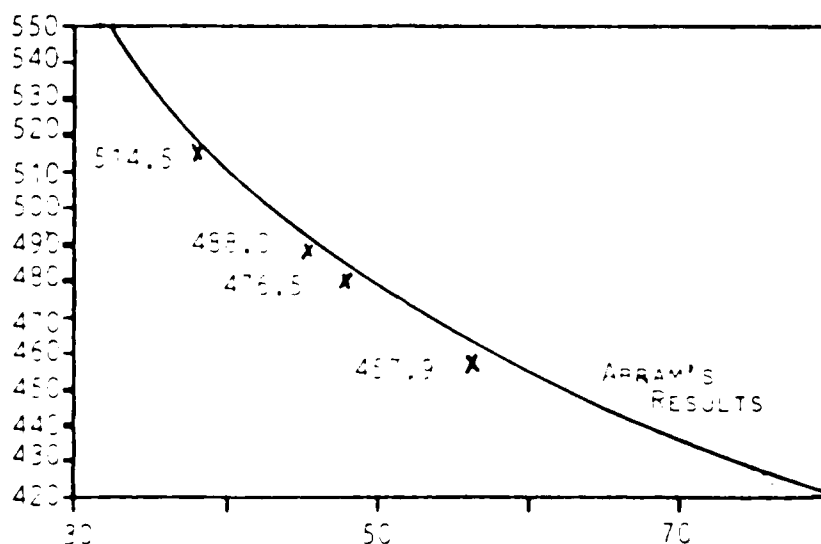NM

Fig. 18. Measured Optical Activity in BSO

The next section of the experiment was to
demonstrate the aberration correcting ability of a PCM. This
was done earlier in fluorescein-doped boric acid glass, but
this time the goal was to produce an image which would better
demonstrate the aberration correction. The setup for this is
pictured in Fig. 19. The wavelength used was 488.0 nm.

41

Several components were added to the system for various reasons. Lens L1 was added to enlarge the image for the camera. Lens L2 was inserted to collect the diffracted light rays into the BSO crystal. Lens L2 had a fairly long focal length and focused the beam to a small diameter at the BSO. Lens L3 was used to change the diameter of the beam to completely fill the crystal.

The beam had to be expanded to illuminate the entire image as well as the crystal. The illumination of crystal was critical in determining how much return would be generated. The visible beam size had to be just slightly smaller than the crystal. Any larger or smaller, the PCW dropped off dramatically. If the beam is larger than the crystal, obviously, some of the beam will be lost, thus decreasing the return. If the beam is smaller than the crystal, several possibilities exist for the decreased efficiency. A saturation point may be reached due to the increased intensity and no more charges are available for movement and thus more intensity cannot create a larger index of refraction change so the diffraction efficiency cannot be increased. Also, when the entire crystal is not illuminated, a space-charge field builds up around the area of interaction, interfering with the action of the diffraction grating.

Photographs of the PCW are shown in Fig. 20 with a.) showing the unaberrated image, b.) showing the image
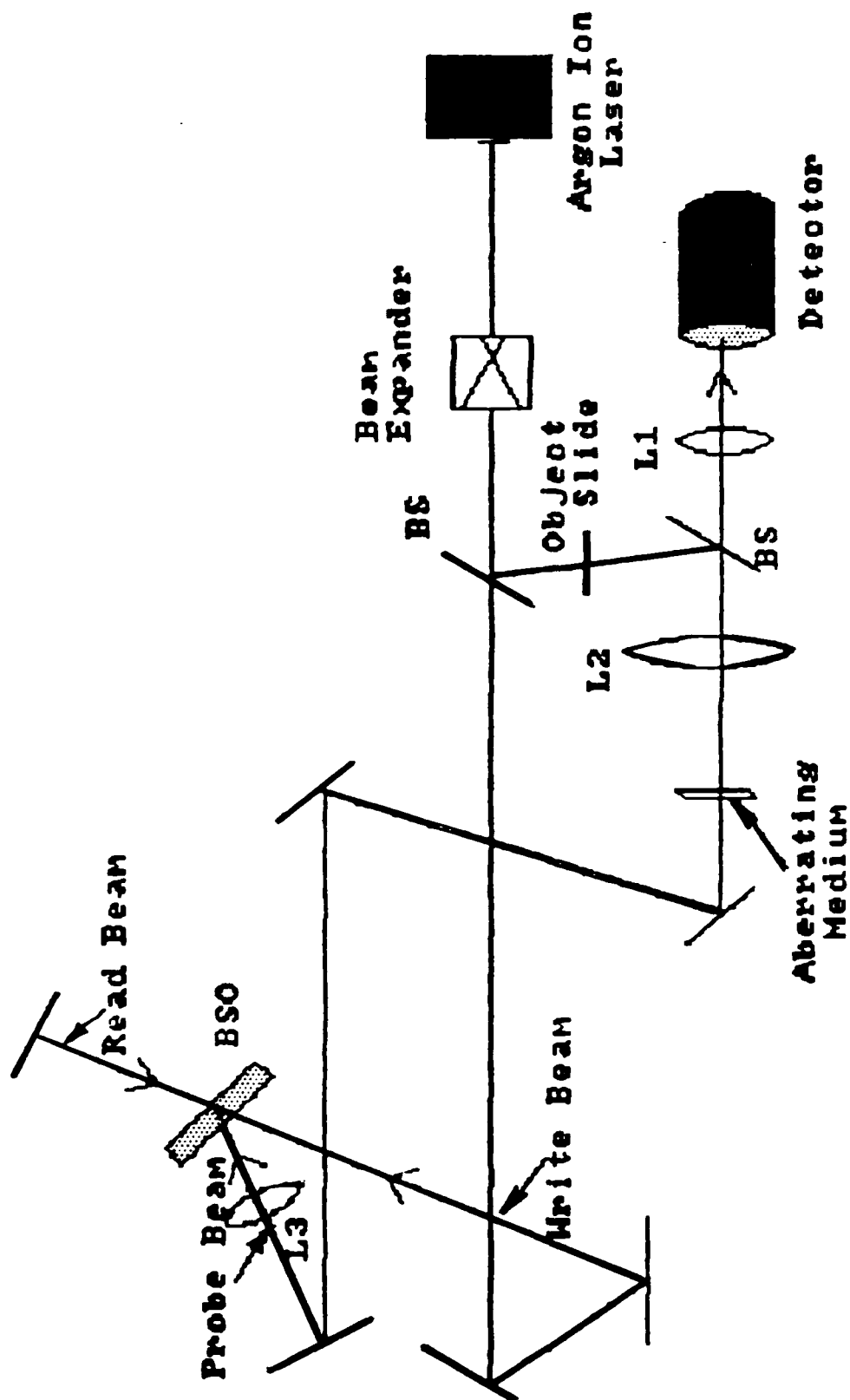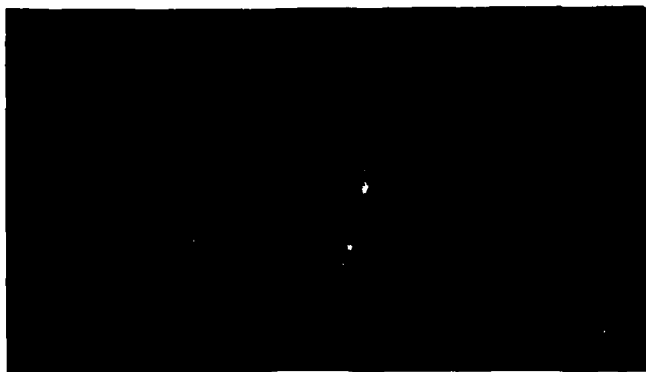
42

Fig. 19. Setup for Image Aberration-Correction via DFWM in BSO

43

Fig. 20.   Photographs of Aberration-Compensation in BSO
        (a.) unaberrated beam, b.) aberrated beam with PCM
replaced with ordinary mirror, and c.) PCM compensated)

aberrated with no PCM correcting the aberration, and

c.) showing the aberrated image compensated for by the PCM.
The aberrator was a microscope slide etched with hydrofluoric
acid.

The next measurement made was the effect of the read
beam upon the efficiency. The wavelength used was 514.5 nm
since it is one of the two higher power wavelengths of the
laser and, of the two, it is the one that shows a
polarization that is different after transmission through the
crystal. The lens and an object slide were removed and a
beam splitter was placed in the write beam to create a
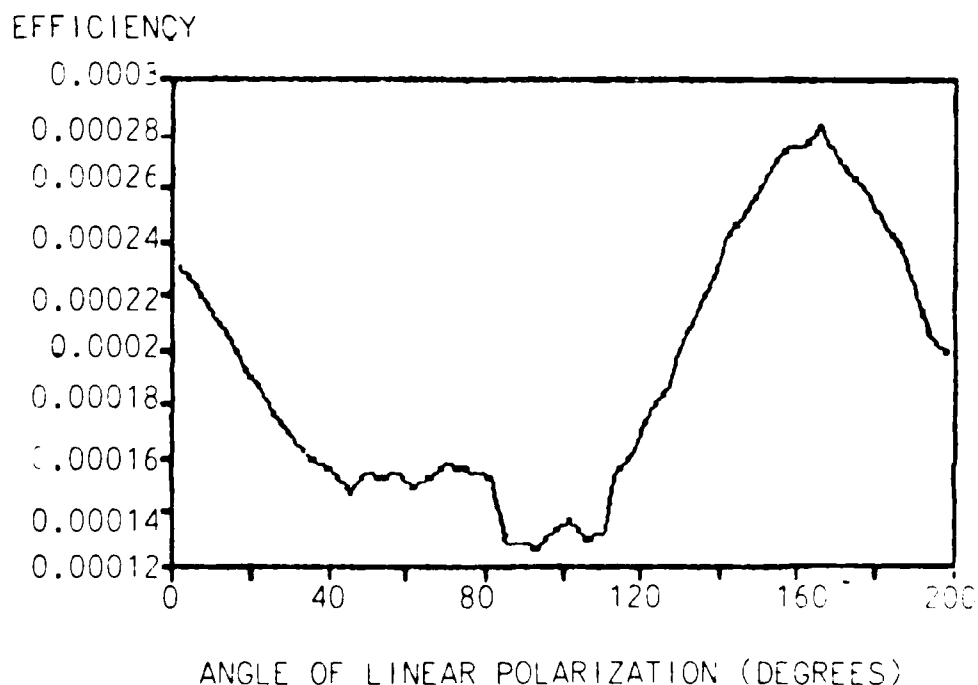separate read beam. A half-wave plate was then placed in the

Fig. 21. Efficiency of Diffraction Grating vs.
Polarization of Read Beam

read beam to rotate the polarization. The polarization of
the write and probe beams was vertical which corresponds to
90 degrees in the graph in Fig. 21.

When the polarization of the read beam is at 45° with
respect to the x' and y' axis of the index ellipsiod as shown
in Fig. 22, the beam "sees" the maximum change index of

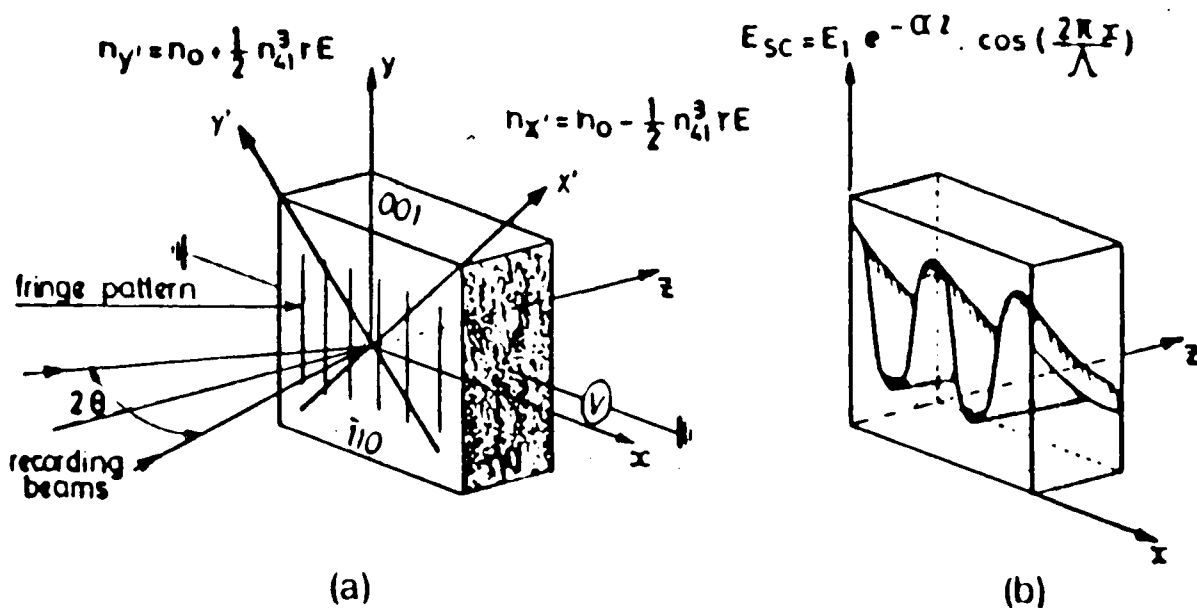(a)   (b)

Fig. 22. BSO Index Ellipsiod and Diffraction Grating
    a.) Crystallographic orientation of cubic BSO crystals
            for maximum diffraction efficiency
    b.) Shape of the photoinduced space charge field in BSO

46

refraction (n r E) which in turn will produce the maximum diffraction efficiency. However, since the polarization rotates (see Fig. 18) as it passes through the crystal the 45° polarization occurs only at certain locations in the crystal, not all through the crystal as ideally would occur. In Fig. 22 b). it can be seen that due to absorption through the crystal, the amplitude of the index grating decreases with distance into the crystal. So, maximum diffraction efficiency should occur when the polarization of the read beam is horizontal or vertical near the front edge of the crystal which would give an additional horizontal or vertical 2 mm back into the crystal. Since the read beam is also attenuated as it passes through the crystal, it is difficult to predict the optimum combination of index grating amplitude and read beam amplitude, i.e. which of the two locations of vertical or horizontal polarization will contribute the most to the diffraction efficiency.

The diffraction efficiency did exhibit a definite dependence upon the polarization of the read beam as seen in Fig. 21. The peak in the diffraction efficiency occurred when the input polarization was at 160° (vertical was at 90°) which produced a horizontal polarization 0.1 mm from the front of the crystal as seen in Fig.23. However, no similar peak in diffraction efficiency occurred when the vertical polarization occurred 0.1 mm from the front of the crystal.
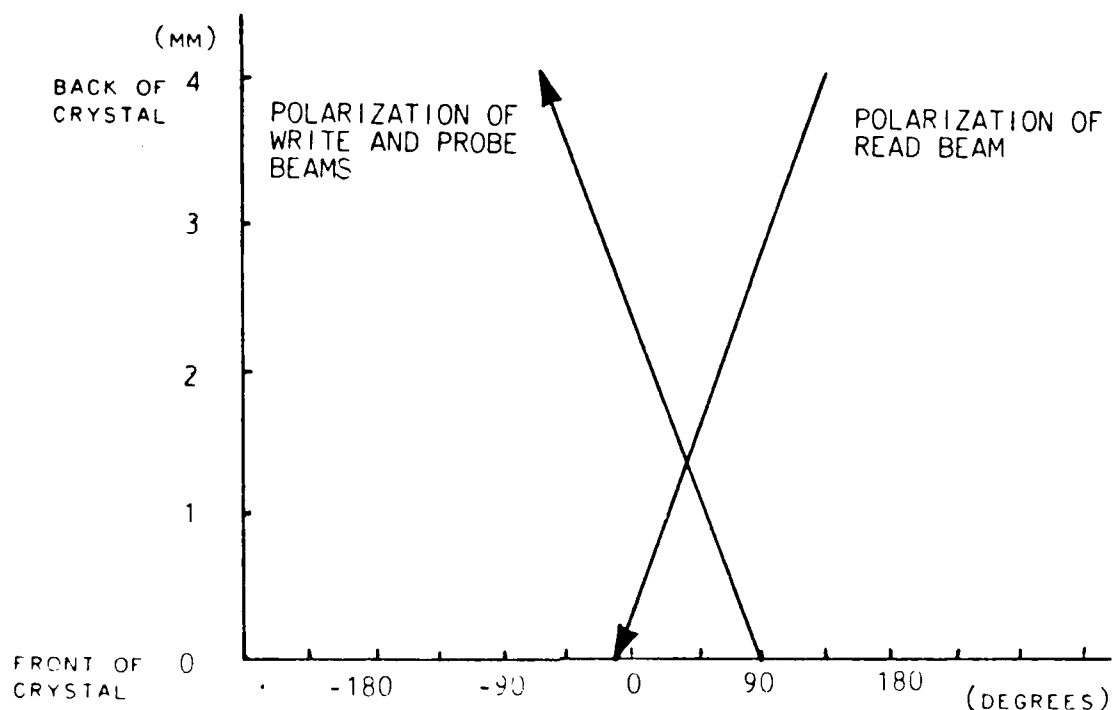
47

Fig. 23.   Polarization of Write and Read Beams Through
the Crystal

The next measurements that were done were angle between

probe and write beam to find maximum efficiency. This was a

difficult measurement to perform because so much "tweaking"

of the optical components was required to optimize each

setting. Also, any path length changes, no matter how small,

changed the efficiency by large amounts. The results are

pictured in Fig. 23. The diffraction efficiency peaked at 28

degrees which corresponds to a grating spacing of 1.06

microns. This peak occurs at a larger spacing than than

published values shown in Fig.23 shown by the dotted line.

The peak should occur near 40° which would make the grating

48

spacing approximately 0.5 microns. However, at this spacing
the sensitivity of the grating to effects of mechanical
instabilities would be critical.

Since the efficiency measured in the experiment was only
one quarter of the published values, it seems likely that
something caused the efficiency not to reach the peak at 0.5
microns, namely, mechanical vibrations that washed out the
grating at the smaller spacings. Also, as when the angle
between the beams increased, the reflection losses at the
surfaces increased, therefore decreasing the measured
efficiency. Anti-reflection coatings on the crystal surfaces
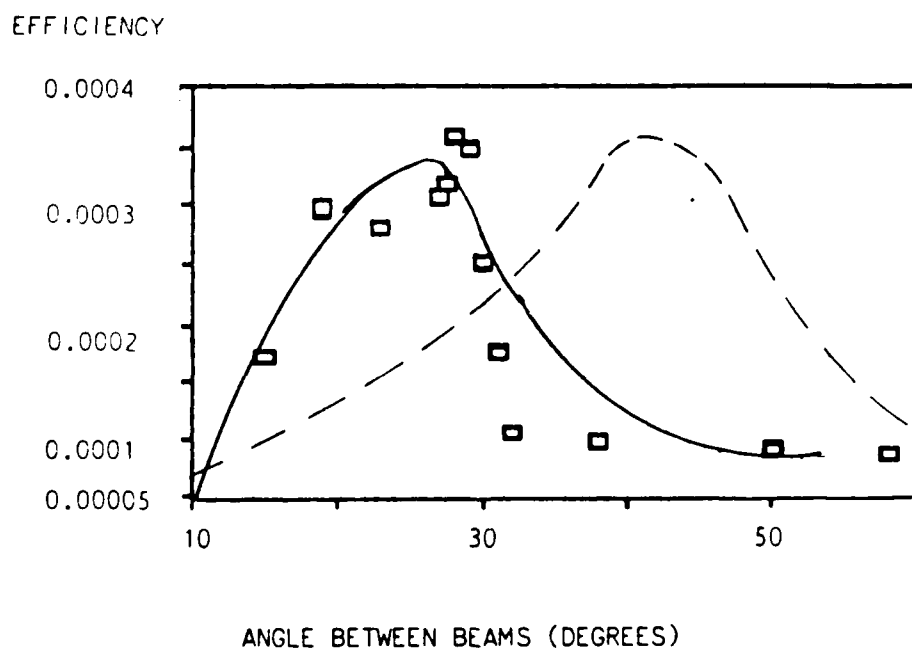would be helpful in eliminating this problem.

EFFICIENCY

ANGLE BETWEEN BEAMS (DEGREES)

Fig. 24. Diffraction Efficiency vs.Angle Between Write and
Probe Beams (Theoretical Values Shown with Dotted Line)

49

The diffraction efficiency is also dependent upon the intensity of the incident beams as seen in Fig. 25. The efficiency peaked at an intensity near .2 mW / cm^2 and tailed off beyond that point due to saturation which is dependent upon the density of trapping centers. Increasing the number of trapping centers during crystal formation would then increase the diffraction efficiency.
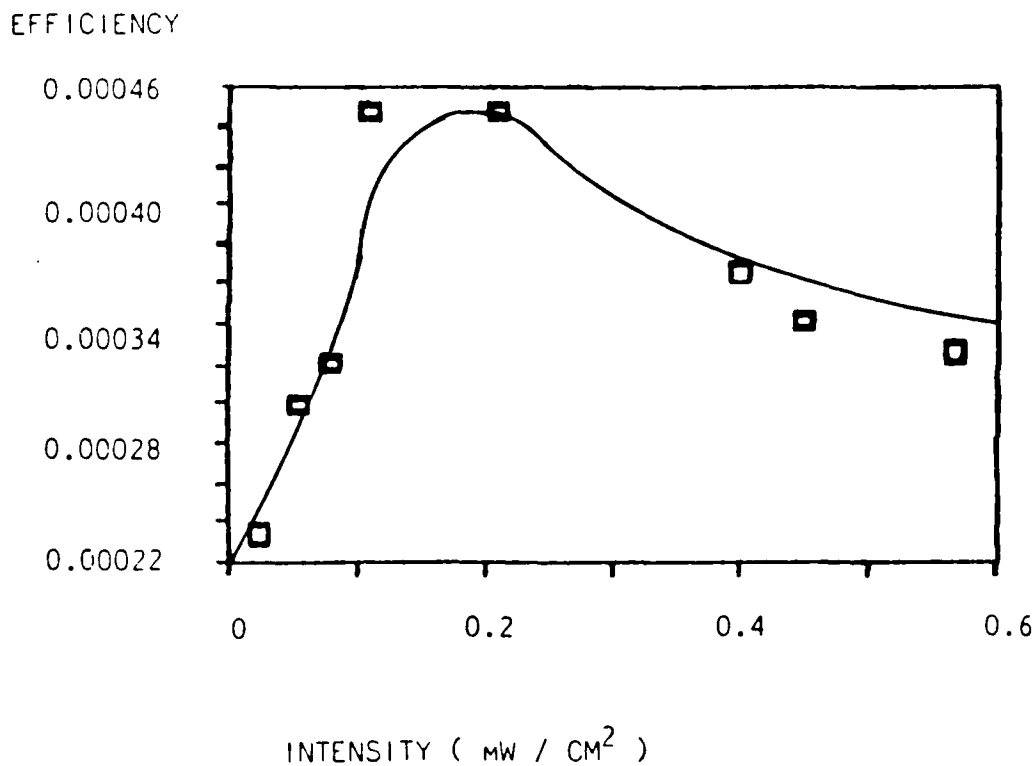
EFFICIENCY

INTENSITY (MW / CM^2)

Fig. 25. Diffraction Efficiency vs. Intensity in BSO

The PCW produced showed a quick response time to the incident beams. At 514.5 nm at 0.8 mW / cm^2 the PCW rose to its full value in 2 seconds, while at 0.14 mW / cm^2 it took

10 seconds to reach its maximum value. At 488.0 nm the
response time was somewhat slower. At 1.8 mW / cm^2 the PCW
took 0.5 seconds to reach its maximum value, while at 0.51 mW
/ cm^2, it took 1.5 seconds. Logically, the higher energy
488.0 nm wavelength should produce quicker response times.
However, the maximum diffraction efficiency at 514.5 nm was
still higher than at 488.0 nm. No overshoot was exhibited in
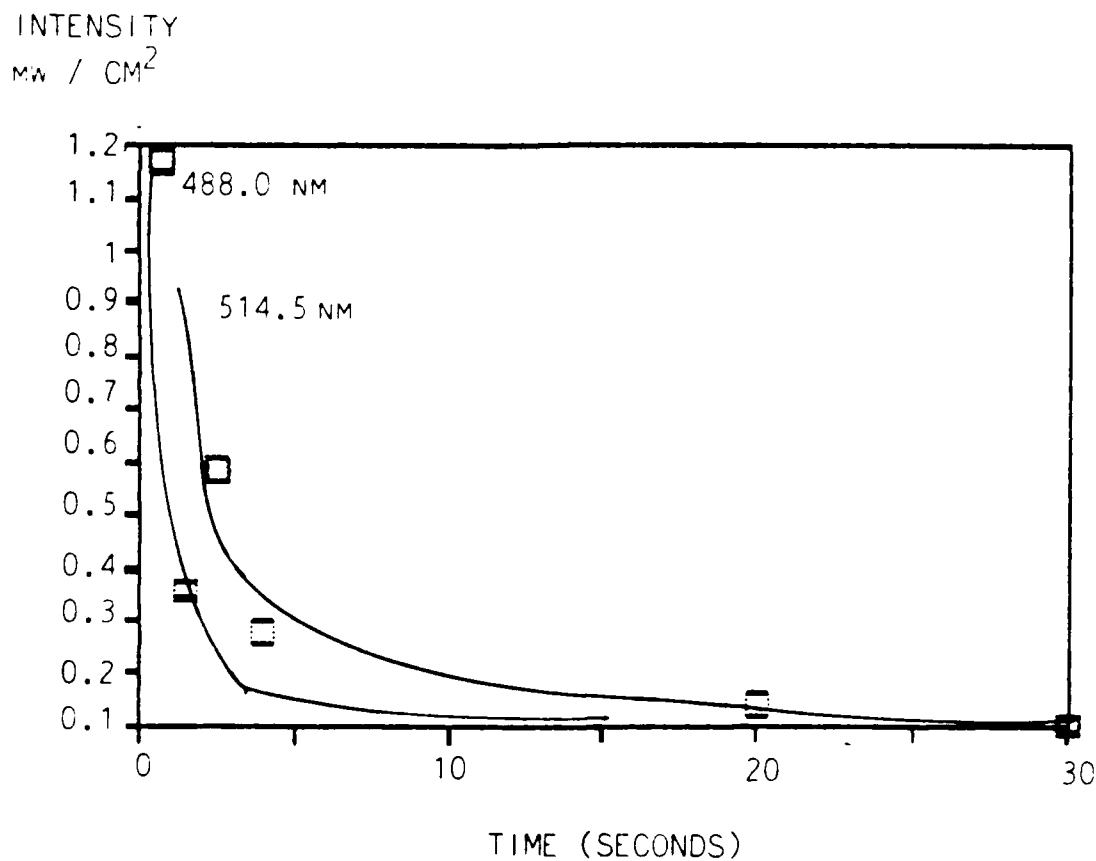BSO as was noted in fluorescein. These results are shown in
Fig. 26.

INTENSITY
MW / CM^2

TIME (SECONDS)

Fig. 26.   Rise Time of PCW in BSO at 488.0 nm and 514.5 nm

D. Two-Wave Mixing in BSO

For the two-wave mixing (TWM) experiments, the BSO crystal was rotated 90 degrees so the c-axis of the crystal was horizontal (in the plane of the incident beams). The various parameters to be measured included angle between the beams, relative power of the beams, and wavelength. The coupling efficiency was then measured as a function of these.

The first test that was done was the determination of the direction of coupling in BSO. The direction of energy transfer was determined to be the opposite of barium titanate which means that the charge carriers are negative according to Feinburg (5:431). The direction of coupling is shown in Fig. 27.
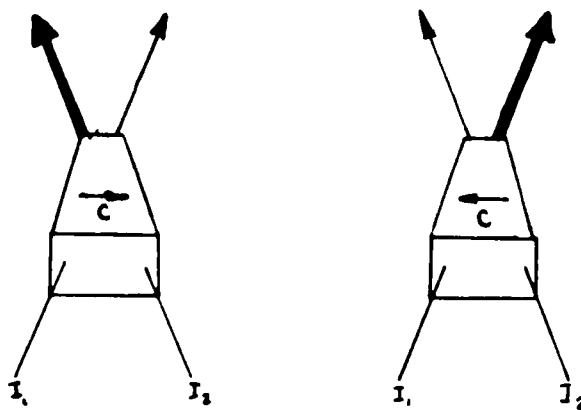

Fig. 27.   Direction of Energy Transfer in BSO

Since the preferred direction of coupling seemed unpredictable due to the isotropic nature of the crystal, tests were done to make sure that the coupling direction would be the same every time. Since subsequent tests might be influenced by a residual grating in the crystal, the crystal was illuminated for 30 minutes between tests with a high intensity mercury lamp. However, the direction of coupling remained the same for every test, so evidently, there is a preferred direction of coupling.

The gain, γ, of the energy transfer is dependent upon the angle between the beams which determines the grating spacing in the BSO. So the next measurement taken was the effect of this angle upon γ. The gain should peak when the spacing is 1 micron, according to Gunter (8:250). Experimentally, no angle dependence could be found however.

The magnitude of the energy transfer also depends upon the ratio of intensities of the two beams. Fig. 28 compares the experimental results with results published by Gunter (8:268). The dotted line again shows Gunter's results.
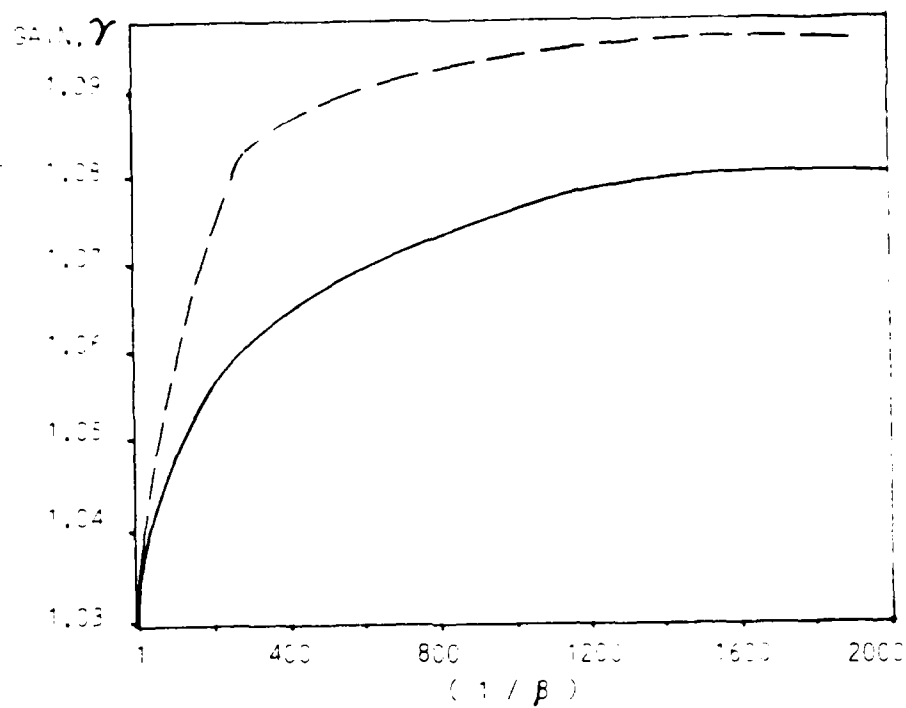
Fig. 28. γ vs Ratio of Intensities in Incident Beams in BSO at 514.5 nm

(8:264)

IV.   CONCLUSIONS AND RECOMMENDATIONS

Phase conjugation was produced in fluorescein-doped boric acid glass and in BSO over a wide range of operating conditions. The maximum diffraction efficiency of fluorescein was higher than BSO--0.0013 to 0.00044, respectively. The maximum diffraction efficiency in fluorescein was produced at a wavelength of 457.9 nm, at an intensity of 49 mW / cm^2, at a β of 0.35 and a grating spacing of 0.72 microns. The maximum diffraction efficiency in BSO was produced at a wavelength of 514.5 nm, at an intensity of 0.2 mW/cm^2, at a β equal to nearly one, and a grating spacing of 1.06 microns. To achieve this maximum efficiency in BSO, the polarization of the read beam must be rotated, prior to striking the crystal, to provide a horizontal polarization at the point in the crystal where the write and probe beams enter the crystal. At higher intensities, the diffraction efficiency decreased. Phase conjugation in fluorescein is not dependent upon orientation of the fluorescein or polarization, if linear, but elliptical polarization decreases the efficiency. The c-axis of BSO must be normal to the plane of incidence of the three beams with polarization of the probe and write beams parallel to the c-axis to produce maximum diffraction efficiency.

No grating spacing dependence could be found in TWM in BSO. The amount of energy transfer was minimal and was

55

difficult to measure exactly. However, the energy transfer showed a dependence upon the ratio between the beams, ß. As ß increased, in the proper crystal orientation, more energy was transferred to the less intense beam.

Fluorescein-doped boric acid glass is an inexpensive, easily obtainable medium for optical phase conjugation at low power levels and exhibits fast response times to input light. Further work should be done to investigate the technique used in making the fluorescein-doped boric acid glass. The thickest sample used produced the greatest efficiency, so if thicker samples could be produced without cracking, efficiency might be increased. Also, samples of higher concentrations of fluorescein should be investigated.

BSO also demonstrated a quick response time to low intensities of incident beams. However, BSO is expensive, difficult to obtain, and shows very low diffraction efficiencies without a transverse voltage applied. Further work should be done to investigate the application of up to 20 KV to BSO for applications in phase conjugation and TWM. The diffraction efficiency of BSO could be greatly increased by applying a voltage transversely as shown in Fig. 4. The speed of BSO response to input radiation shows promise for the aberration correction of moderately varying aberrating media.

Bibliography

1. Abrams, R. L. and R. C. Lind. "Degenerate Four-Wave Mixing in Absorbing Media,"Optics Letters, 2: 94-96 (April 1978).

2. Abrams, S. C. and C. Svensson. "Crystal Chirality and Optical Rotation Sense in Isomorphous Bi12SiO20 and Bi12GeO20," Solid State Communications, 30: 293-295 (May 1979).

3. Bar-Joseph, Israel and Yaron Silverburg. "Real Time Holography Through Triplet State Absorption in Organic Dyes," Optics Communications, 41: 455-458 (May 1982).

4. Feinburg, Jack, D. Heiman, A. R. Tanguay, Jr., and R. W. Hellwarth. "Photorefractive Effects and Light-Induced Charge Migration in Barium Titanate," Journal of Applied Physics, 51: 1297-1305 (March 1980)

5. Fisher, Robert A. Optical Phase Conjugation. New York: Academic Press, 1983.

6. Fujiwara, H. and K. Nakagawa. "Phase Conjugation in Fluorescein Film by Degenerate Four-Wave Mixing and Holographic Process," Optics Communications, 55: 386-390 (October 1985).

7. Giuliano, Concetto R. "Applications of Optical Phase Conjugation," Physics Today, 27-35 (April 1981).

8. Günter, P. "Holography, Coherent Light Amplification and Optical Phase Conjugation with Photorefractive Materials," Physics Reports, 93: 199-299 (1982).

9. Herriau, J. P., J. P. Huignard, and P. Aubourg. "Some Polarization Properties of Volume Holograms in Bi12SiO20 Crystals and Application," Applied Optics, 17: 1851-1852 (June 1978).

10. Huignard, J. P., J. P. Herriau, and G. Rivet. "Phase Conjugation and Spatial-Frequency Dependence of Wavefront Reflectivity in Bi12SiO20 Crystals," Optics Letters, 5: 102-104 (March 1980).

11. -----. "Phase-Conjugate Wavefront Generation via Real Time Holography in Bi12SiO20 Crystals," Optics Letters, 4: 21-23 (January 1978).

12. Kramer, Mark A., Wayne R. Tompkins, and Robert W. Boyd. "Nonlinear-Optical Interactions in Fluorescein-Doped Boric Acid Glass," Physical Review, 34: 2026-2031 (September 1986).

13. Pepper, David M. "Nonlinear Optical Phase Conjugation", Optical Engineering, 21: 156-181 (March/April 1982).

14. -----. "Applications of Optical Phase Conjugation," Scientific American, 74-83 (January 1986).

15. Ryan, James R. Optical Phase Conjugation via Four-Wave Mixing via Four-Wave Mixing, MS thesis, Naval Postgraduate School, Monterey, California, March 1986 (AD-A168908).

16. Silverburg, Y. and I. Bar-Joseph. "Low Power Phase Conjugation in Thin Films of Saturable Absorbers," Optics Communications, 39: 265-268 (October 1981).

17. Todorov, T., L. Nikolova, N. Tomova, and V. Dragostinova. "Photochroism and Dynamic Holographic Recording in a Rigid Solution of Fluorescein," Optical and Quantem Electronics, 13: 209-215 (1981).
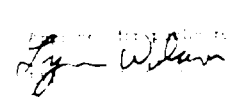
VITA

Captain Phillip R. Leatherman was born on 2 August 1957 in Baxter Springs, Kansas. He graduated from high school in Eureka, Illinois, in 1975 and attended Olivet Nazarene University, from which he received the degree of Bachelor of Arts in chemistry in May 1979. Upon graduation, he was employed by Moline Paint Manufacturing (Moline, Illinois) as a research chemist. In July 1980, he received a commission in the USAF through the OTS program. Upon commissioning, he entered the School of Engineering, Air Force Institute of Technology, from which he received the degree of Bachelor of Science in electrical engineering. He then served at Hill AFB, Utah, as flight simulator engineer in Materiel Management until entering the School of Engineering, Air Force Institute of Technology, in June 1986.

Permanent address: 1099 Beaver Valley Road
Beavercreek, Ohio 45385

ADA189716

REPORT DOCUMENTATION PAGE

Form Approved
OMB No 0704-0188

1a REPORT SECURITY CLASSIFICATION UNCLASSIFIED	1b RESTRICTIVE MARKINGS
2a. SECURITY CLASSIFICATION AUTHORITY	3 DISTRIBUTION/AVAILABILITY OF REPORT APPROVED FOR PUBLIC RELEASE; DISTRIBUTION UNLIMITED.
2b DECLASSIFICATION DOWNGRADING SCHEDULE	

4 PERFORMING ORGANIZATION REPORT NUMBER(S) AFIT/GEO/ENP/87D-2	5 MONITORING ORGANIZATION REPORT NUMBER(S)

6a. NAME OF PERFORMING ORGANIZATION School of Engineering	6b OFFICE SYMBOL (If applicable) AFIT/EN	7a NAME OF MONITORING ORGANIZATION

6c ADDRESS (City, State, and ZIP Code) Air Force Institute of Technology Wright-Patterson AFB, OH 45433-6583	7b ADDRESS (City, State, and ZIP Code)

8a. NAME OF FUNDING/SPONSORING ORGANIZATION	8b OFFICE SYMBOL (If applicable)	9 PROCUREMENT INSTRUMENT IDENTIFICATION NUMBER

8c. ADDRESS (City, State, and ZIP Code)	10 SOURCE OF FUNDING NUMBERS			
	PROGRAM ELEMENT NO	PROJECT NO	TASK NO	WORK UNIT ACCESSION NO

11 TITLE (Include Security Classification)
NONLINEAR OPTICAL PHASE CONJUGATION IN FLUORESCEIN AND BISMUTH SILICATE (BSO)
Thesis Chairman: Won B. Roh, Professor of Engineering Physics

12 PERSONAL AUTHOR(S)
Phillip B. Weatherman, B.A., B.S., Capt, USAF

13a TYPE OF REPORT MS Thesis	13b TIME COVERED FROM 6/87 to 12/87	14 DATE OF REPORT (Year, Month, Day) 1987 Dec 7	15 PAGE COUNT 67

16 SUPPLEMENTARY NOTATION

17	COSATI CODES		18 SUBJECT TERMS (Continue on reverse if necessary and identify by block number) OPTICAL PHASE CONJUGATION, BSO, FLUORESCEIN, BISMUTH SILICATE, NONLINEAR OPTICAL PHASE CONJUGATION
FIELD	GROUP	SUB-GROUP	

19 ABSTRACT (Continue on reverse if necessary and identify by block number)

SEE REVERSE.

Approved for public release: IAW AFR 190-1

Lynn Wilson 24 Feb 88

20 DISTRIBUTION/AVAILABILITY OF ABSTRACT [ ] UNCLASSIFIED/UNLIMITED [ ] SAME AS RPT [ ] DTIC USERS	21 ABSTRACT SECURITY CLASSIFICATION UNCLASSIFIED
22a NAME OF RESPONSIBLE INDIVIDUAL	22b TELEPHONE (Include Area Code) (513) 255-2012	22c OFFICE SYMBOL AFIT/EN

DD Form 1473, JUN 86   Previous editions are obsolete   SECURITY CLASSIFICATION OF THIS PAGE

19. The goal of the experiment was to produce nonlinear optical phase conjugation (NOPC) in fluorescein-doped boric acid glass and in BSO, and to use two-wave mixing (TWM) in BSO to transfer energy between laser beams. Next, the parameters that affect these processes were to be examined. The parameters measured for phase conjugation were the power and intensity of the various beams, angles between the beams, orientation of the BSO crystal, sample thickness and concentration, polarization and wavelength of the incident beams. An Argon Ion and a HeCd laser were used in the experiment. Phase conjugation was produced in BSO at all wavelengths available; 441.6 nm, 457.9 nm, 476.5 nm, 488.0 nm, and 514.5 nm. In fluorescein-doped boric acid, phase conjugation was produced at all wavelengths but 514.5 nm. The maximum diffraction efficiency of shown in fluorescein was higher than in BSO--0.13 % to 0.044 %. The maximum diffraction efficiency in fluorescein was produced at a wavelength of 457.9 nm, at an intensity of 49 mW / cm^2, and a grating spacing of 0.72 μm. The maximum diffraction efficiency in BSO was produced at a wavelength of 457.9 nm, at an intensity of 0.2 mW / cm^2, at a ß equal to 1, and a grating spacing of 1.06 μm. In two-wave mixing experiments the maximum energy transfer was 7.5 % of the weaker beam and occurred when the c-axis was in the plane of the beams and ß was equal to 2000.

END

DATE

FILMED

APRIL

1988

DTIC